Available online at www.sciencedirect.com
SCIENCE DIRECT
ELSEVIER
International Journal of Solids and Structures 43 (2006) 2761–2798
INTERNATIONAL JOURNAL OF SOLIDS and STRUCTURES
www.elsevier.com/locate/ijsolstr

Interactions due to mechanical/thermal sources in a micropolar thermoelastic medium possessing cubic symmetry

Rajneesh Kumar [a,*], Praveen Ailawalia [b]

[a] Department of Mathematics, Kurukshetra University, Kurukshetra, Haryana 136 119, India
[b] Department of Applied Sciences, Institute of Engineering and Emerging Technologies, Makhnumajra, Baddi, Distt. Solan, Himachal Pradesh 173 205, India

Received 27 January 2005
Available online 18 January 2006

Abstract

The present problem is the deformation of micropolar thermoelastic solids with cubic symmetry under the influence of various sources acting on the plane surface. Analytic expressions for displacement components, microrotation, force stress, couple stress, and temperature distribution are obtained in the physical domain for Lord–Shulman (L–S) and Green–Lindsay (G–L) theories of thermoelasticity by applying integral transforms. A numerical inversion technique has been applied to obtain the solution in the physical domain. The numerical results are presented graphically for a particular model.

Keywords: Micropolar thermoelastic solid; Cubic symmetry; Couple stress; Microrotation; Thermoelasticity; Integral transform

1. Introduction

The classical theory of heat conduction predicts infinite speed of heat transportation, if a material that conducts heat is subjected to a thermal disturbance, which contradicts the physical facts. Lord and Shulman (1967) incorporated a flux rate term into the Fouriers law of heat conduction and formulated a generalized theory admitting finite speed for thermal signals. Green and Lindsay (1972) have developed a temperature-rate-dependent thermoelasticity by including temperature rate among the constitutive variables, which does not violate the classical Fouriers law of heat conduction when the body under consideration has a center of symmetry, and this theory also predicts a finite speed of heat propagation. Green and Naghdi (1991) established a new thermomechanical theory of deformable media that uses a general entropy balance. The generalized thermoelasticity theories are supposed to be more realistic than the conventional theory in dealing with practical problems involving very large heat fluxes and/or short time intervals, such as those occurring in laser units and energy channels.

* Corresponding author.
E-mail addresses: rajneesh_kuk@rediffmail.com (R. Kumar), praveen_2117@rediffmail.com (P. Ailawalia).

0020-7683/$ - see front matter © 2005 Published by Elsevier Ltd.
doi:10.1016/j.ijsolstr.2005.11.002

The classical theory of elasticity is inadequate to represent the behavior of some modern engineering structures such as polycrystalline materials and materials with fibrous or coarse grain. The study of these materials requires incorporation of theory of oriented media. "Micropolar elasticity", termed by Eringen (1966), is used to describe the deformation of elastic media with oriented particles. A micropolar continuum is a collection of interconnected particles in the form of small rigid bodies undergoing both translational and rotational motions. The force at a point of a surface element of bodies of these materials is completely characterized by a stress vector and a couple stress vector at that point.

Following various methods, the elastic fields of various loadings, inclusion and inhomogeneity problems, and interaction energy of point defects and dislocation arrangement have been discussed extensively in the past. Generally all materials have elastic anisotropic properties, which means that the mechanical behavior of an engineering material is characterized by the direction dependence. However, the three-dimensional study of an anisotropic material is much more complicated than the isotropic one, due to the large number of elastic constants involved in the calculation. In recent years the elastodynamic response of anisotropic continua has received the attention of several researchers. In particular, transversely isotropic and orthotropic materials, which may not be distinguished from each other in plane strain and plane stress, have been more regularly studied. Kumar and Choudhary (2002a,b, 2003) discussed different types of problems in an orthotropic micropolar continua.

A wide class of crystals such as W, Si, Cu, Ni, Fe, Au, and Al, which are frequently used substances, belong to cubic materials. The cubic materials have nine planes of symmetry whose normals are on the three coordinate axes and on the coordinate planes making an angle of $\pi/4$ with the coordinate axes. With the chosen coordinate system along the crystalline directions, the mechanical behavior of a micropolar cubic crystal can be characterized by four independent elastic constants.

To understand the crystal elasticity of a cubic material, Chung and Buessem (1967) presented a convenient method to describe the degree of the elasticity anisotropy in a given cubic crystal. Later Lie and Koehler (1968) used a Fourier expansion scheme to calculate the stress fields caused by a unit force in a cubic crystal. Steeds (1973) gave a complete discussion of the displacements, stresses, and energy factors of the dislocations for two-dimensional anisotropic materials. Boulanger and Hayes (2000) investigated inhomogeneous plane waves in cubic elastic materials. Bertram et al. (2000) discussed generation of discrete isotropic orientation distributions for linear elastic cubic crystals. Kobayashi and Giga (2001) investigated anisotropy and curvature effects for growing crystals. Domanski and Jablonski (2001) studied resonances of nonlinear elastic waves in cubic crystal. Destrade (2001) considered the explicit secular equation for surface acoustic waves in monoclinic elastic crystals. Zhou and Ogawa (2002) investigated elastic solutions for a solid rotating disk with cubic anisotropy. Minagawa et al. (1981) discussed the propagation of plane harmonic waves in a cubic micropolar medium. Recently Kumar and Rani (2003) studied time-harmonic sources in a thermally conducting cubic crystal. However, no attempt has been made to study source problems in micropolar thermoelastic solids with cubic symmetry.

The results of the problem may be applied to a wide class of geophysical problems involving temperature change. The physical applications are encountered in the context of problems such as ground explosions and oil industries. This problem is also useful in the field of geomechanics, where the interest is in various phenomenon occurring in earthquakes and measurement of displacements, stresses, and temperature field due to the presence of certain sources. The present investigation seeks to determine the components of displacement, microrotation, and stress in a micropolar thermoelastic medium with cubic symmetry due to mechanical/thermal sources. The solution is obtained by introducing potential functions after employing an integral transformation technique. The integral transforms are inverted using a numerical method.

2. Problem formulation

We consider a homogeneous, micropolar thermoelastic solid half-space with cubic symmetry. We consider a rectangular coordinate system (x, y, z) having origin on the surface $y = 0$ and y-axis pointing vertically into the medium. A normal force/thermal source is assumed to be acting at the origin of the rectangular Cartesian coordinates. If we restrict our analysis to plane strain parallel to the xy-plane with displacement vector $\mathbf{u} = (u_1, u_2, 0)$ and microrotation vector $\boldsymbol{\phi} = (0, 0, \phi_3)$ then the field equations and constitutive relations for a

micropolar thermoelastic solid with cubic symmetry in the absence of body forces, body couples, and heat sources can be written following the equations given by Minagawa et al. (1981), Lord and Shulman (1967), and Green and Lindsay (1972) as

$$A_1\frac{\partial^2 u_1}{\partial x^2}+A_3\frac{\partial^2 u_1}{\partial y^2}+(A_2+A_4)\frac{\partial^2 u_2}{\partial x\,\partial y}+(A_3-A_4)\frac{\partial \phi_3}{\partial y}-v\frac{\partial}{\partial x}\left(T+\delta_{2k}t_1\frac{\partial T}{\partial t}\right)=\rho\frac{\partial^2 u_1}{\partial t^2}, \tag{1}$$

$$A_3\frac{\partial^2 u_2}{\partial x^2}+A_1\frac{\partial^2 u_2}{\partial y^2}+(A_2+A_4)\frac{\partial^2 u_1}{\partial x\,\partial y}-(A_3-A_4)\frac{\partial \phi_3}{\partial x}-v\frac{\partial}{\partial y}\left(T+\delta_{2k}t_1\frac{\partial T}{\partial t}\right)=\rho\frac{\partial^2 u_2}{\partial t^2}, \tag{2}$$

$$B_3\nabla^2\phi_3+(A_3-A_4)\left(\frac{\partial u_2}{\partial x}-\frac{\partial u_1}{\partial y}\right)-2(A_3-A_4)\phi_3=\rho j\frac{\partial^2\phi_3}{\partial t^2}, \tag{3}$$

$$K^*\nabla^2 T=\rho C^*\left(\frac{\partial T}{\partial t}+t_0\frac{\partial^2 T}{\partial t^2}\right)+vT_0\left(\frac{\partial}{\partial t}+t_0\delta_{1k}\frac{\partial^2}{\partial t^2}\right)\left(\frac{\partial u_1}{\partial x}+\frac{\partial u_2}{\partial y}\right), \tag{4}$$

$$t_{22}=A_2\frac{\partial u_1}{\partial x}+A_1\frac{\partial u_2}{\partial y}-v\left(T+\delta_{2k}t_1\frac{\partial T}{\partial t}\right), \tag{5}$$

$$t_{21}=A_4\left(\frac{\partial u_2}{\partial x}-\phi_3\right)+A_3\left(\frac{\partial u_1}{\partial y}+\phi_3\right), \tag{6}$$

$$m_{23}=B_3\frac{\partial\phi_3}{\partial y}, \tag{7}$$

where t_{22}, t_{21}, m_{23} are the components of normal force stress, tangential force stress, and tangential couple stress, respectively. A_1, A_2, A_3, A_4, and B_3 are characteristic constants of the material; $v=(A_1+2A_2)\alpha_T$; α_T is the coefficient of linear expansion; ρ is the density and j is the microinertia; K^* is the coefficient of thermal conductivity; C^* is the specific heat at constant strain; and t_0 and t_1 are the thermal relaxation times. δ_{ik} $(i=1,2)$ is the Kronecker delta. For Lord–Shulman (L–S) theory $t_1=0$ and $k=1$, and for Green–Lindsay (G–L) theory $t_1>0$, $k=2$, and $\nabla^2=\frac{\partial^2}{\partial x^2}+\frac{\partial^2}{\partial y^2}$.

Introducing dimensionless variables defined by

$$\begin{aligned}&x'=\frac{\omega}{c_1}x,\qquad y'=\frac{\omega}{c_1}y,\qquad \phi_3'=\frac{\rho c_1^2}{vT_0}\phi_3,\qquad \{t_{22}',t_{21}'\}=\frac{\{t_{22},t_{21}\}}{vT_0},\qquad u_1'=\frac{\rho c_1\omega}{vT_0}u_1,\\ &u_2'=\frac{\rho c_1\omega}{vT_0}u_2,\qquad m_{23}'=\frac{\omega}{c_1vT_0}m_{23},\qquad t'=\omega t,\qquad t_1'=\omega t_1,\qquad t_0'=\omega t_0,\qquad a'=\frac{\omega}{c_1}a,\\ &T'=\frac{T}{T_0},\qquad h'=\frac{c_1}{\omega}h,\qquad F'=\frac{F}{vT_0},\end{aligned} \tag{8}$$

where $\omega=\rho C^*c_1^2/K^*$, $\varepsilon=v^2T_0/\rho\omega K^*$, and $c_1^2=\frac{A_1}{\rho}$, into Eqs. (1)–(4) we obtain (after dropping the primes)

$$\frac{\partial^2 u_1}{\partial x^2}+\frac{A_3}{\rho c_1^2}\frac{\partial^2 u_1}{\partial y^2}+\frac{(A_2+A_4)}{\rho c_1^2}\frac{\partial^2 u_2}{\partial x\,\partial y}+\frac{(A_3-A_4)}{\rho c_1^2}\frac{\partial\phi_3}{\partial y}-\frac{\partial}{\partial x}\left(T+\delta_{2k}t_1\frac{\partial T}{\partial t}\right)=\frac{\partial^2 u_1}{\partial t^2}, \tag{9}$$

$$\frac{A_3}{\rho c_1^2}\frac{\partial^2 u_2}{\partial x^2}+\frac{\partial^2 u_2}{\partial y^2}+\frac{(A_2+A_4)}{\rho c_1^2}\frac{\partial^2 u_1}{\partial x\,\partial y}-\frac{(A_3-A_4)}{\rho c_1^2}\frac{\partial\phi_3}{\partial x}-\frac{\partial}{\partial y}\left(T+\delta_{2k}t_1\frac{\partial T}{\partial t}\right)=\frac{\partial^2 u_2}{\partial t^2}, \tag{10}$$

$$\nabla^2\phi_3+\frac{(A_3-A_4)c_1^2}{B_3\omega^2}\left(\frac{\partial u_2}{\partial x}-\frac{\partial u_1}{\partial y}\right)-\frac{2(A_3-A_4)c_1^2}{B_3\omega^2}\phi_3=\frac{\rho jc_1^2}{B_3}\frac{\partial^2\phi_3}{\partial t^2}, \tag{11}$$

$$\nabla^2 T=\frac{\rho C^*c_1^2}{K^*\omega}\left(\frac{\partial T}{\partial t}+t_0\frac{\partial^2 T}{\partial t^2}\right)+\varepsilon\left(\frac{\partial}{\partial t}+t_0\delta_{1k}\frac{\partial^2}{\partial t^2}\right)\left(\frac{\partial u_1}{\partial x}+\frac{\partial u_2}{\partial y}\right). \tag{12}$$

Introducing potential functions defined by

$$u_1=\frac{\partial q}{\partial x}+\frac{\partial\Psi}{\partial y},\qquad u_2=\frac{\partial q}{\partial y}-\frac{\partial\Psi}{\partial x}, \tag{13}$$

into Eqs. (9)–(12), where $q(x,y,t)$ and $\Psi(x,y,t)$ are scalar potential functions, we obtain

$$\left[\frac{\partial^2}{\partial x^2}+a_{11}\frac{\partial^2}{\partial y^2}-\frac{\partial^2}{\partial t^2}\right]q-\left(1+t_1\delta_{2k}\frac{\partial}{\partial t}\right)T=0, \tag{14}$$

$$\left[a_{12}\frac{\partial^2}{\partial x^2}+a_{13}\frac{\partial^2}{\partial y^2}-\frac{\partial^2}{\partial t^2}\right]\Psi+a_{14}\phi_3=0, \tag{15}$$

$$a_{15}\nabla^2\Psi+\left[\nabla^2+2a_{15}-a_{16}\frac{\partial^2}{\partial t^2}\right]\phi_3=0, \tag{16}$$

$$\varepsilon\left[\frac{\partial^2}{\partial t^2}+t_0\delta_{1k}\frac{\partial^2}{\partial t^2}\right]\nabla^2 q+\left[\frac{\partial}{\partial t}+t_0\frac{\partial^2}{\partial t^2}-\nabla^2\right]T=0, \tag{17}$$

where

$$\begin{aligned} &a_{11}=\frac{A_2+A_3+A_4}{\rho c_1^2}, \qquad a_{12}=1-\frac{(A_2+A_4)}{\rho c_1^2}, \qquad a_{13}=\frac{A_3}{\rho c_1^2},\\ &a_{14}=\frac{A_3-A_4}{\rho c_1^2}, \qquad a_{15}=\frac{(A_4-A_3)c_1^2}{B_3\omega^2}, \qquad a_{16}=\frac{\rho j c_1^2}{B_3}. \end{aligned} \tag{18}$$

Applying the Laplace transform with respect to time t defined by

$$\{\bar{q},\overline{\Psi},\overline{T},\bar{\phi}_3\}(x,y,p)=\int_0^\infty\{q,\Psi,T,\phi_3\}(x,y,t)\mathrm{e}^{-pt}\,\mathrm{d}t, \tag{19}$$

and then the Fourier transform with respect to x defined by

$$\{\tilde{q},\widetilde{\Psi},\widetilde{T},\tilde{\phi}_3\}(\xi,y,p)=\int_{-\infty}^\infty\{\bar{q},\overline{\Psi},\overline{T},\bar{\phi}_3\}(x,y,p)\mathrm{e}^{\mathrm{i}\xi x}\,\mathrm{d}x, \tag{20}$$

to Eqs. (14)–(17) and eliminating $\widetilde{T}$ and $\tilde{\phi}_3$ from the resulting expressions, we get

$$\left[\frac{\mathrm{d}^4}{\mathrm{d}y^4}+A^*\frac{\mathrm{d}^2}{\mathrm{d}y^2}+B^*\right]\tilde{q}=0, \tag{21}$$

$$\left[\frac{\mathrm{d}^4}{\mathrm{d}y^4}+C^*\frac{\mathrm{d}^2}{\mathrm{d}y^2}+D^*\right]\widetilde{\Psi}=0, \tag{22}$$

where

$$\begin{aligned} A^*&=-\frac{1}{a_{11}}[(\xi^2+p^2)+a_{11}(p+t_0p^2+\xi^2)+\varepsilon(p+t_0\delta_{1k}p^2)(1+t_1\delta_{2k}p)],\\ B^*&=\frac{1}{a_{11}}[(\xi^2+p^2)(p+t_0p^2+\xi^2)+\varepsilon\xi^2(p+t_0\delta_{1k}p^2)(1+t_1\delta_{2k}p)],\\ C^*&=-\left[(\xi^2+a_{16}p^2-2a_{15})+\frac{1}{a_{13}}(a_{12}\xi^2+p^2)+\frac{a_{14}a_{15}}{a_{13}}\right],\\ D^*&=\frac{1}{a_{13}}[(a_{12}\xi^2+p^2)(\xi^2+a_{16}p^2-2a_{15})+a_{14}a_{15}\xi^2]. \end{aligned} \tag{23}$$

The roots of Eqs. (21) and (22) are given by

$$q_{1,2}^2=\frac{-A^*\pm\sqrt{A^{*2}-4B^*}}{2}, \qquad q_{3,4}^2=\frac{-C^*\pm\sqrt{C^{*2}-4D^*}}{2}. \tag{24}$$

The solutions of Eqs. (21) and (22) satisfying radiation conditions are given by

$$\tilde{q} = D_1 \exp(-q_1 y) + D_2 \exp(-q_2 y), \tag{25}$$

$$\widetilde{\Psi} = D_3 \exp(-q_3 y) + D_4 \exp(-q_4 y), \tag{26}$$

$$\widetilde{T} = a_1^* D_1 \exp(-q_1 y) + a_2^* D_2 \exp(-q_2 y), \tag{27}$$

$$\tilde{\phi}_3 = a_3^* D_3 \exp(-q_3 y) + a_4^* D_4 \exp(-q_4 y), \tag{28}$$

where

$$a_n^* = \frac{a_{11} q_n^2 - (\xi^2 + p^2)}{1 + t_1 \delta_{2k} p}, \quad a_\Theta^* = \frac{1}{a_{14}} (a_{12} \xi^2 + p^2 - a_{13} q_\Theta^2), \qquad n = 1, 2, \ \ \Theta = 3, 4. \tag{29}$$

3. Boundary conditions

3.1. Mechanical force on the surface of a half-space

The boundary conditions on the surface $y = 0$ are

$$t_{22} = -F \Psi_1(x) \delta(t), \qquad t_{21} = 0, \qquad m_{23} = 0, \qquad \frac{\partial T}{\partial y} + hT = 0, \tag{30}$$

where $\delta(t)$ is the Dirac delta function, $\Psi_1(x)$ specify the vertical traction distribution function along the x-axis, and h is the heat transfer coefficient, where $h \to \infty$ for an isothermal boundary and $h \to 0$ for an insulated boundary.

Applying Laplace and Fourier transforms defined by (19) and (20) to the boundary conditions (30) and using (5)–(8), (13) and (25)–(28), we get the expressions for displacement components, microrotation, force stress, couple stress, and temperature distribution for a micropolar thermoelastic solid with cubic symmetry as

$$\tilde{u}_1 = -\frac{1}{\Delta} [\mathrm{i}\xi \{\Delta_1 \exp(-q_1 y) + \Delta_2 \exp(-q_2 y)\} + q_3 \Delta_3 \exp(-q_3 y) + q_4 \Delta_4 \exp(-q_4 y)], \tag{31}$$

$$\tilde{u}_2 = -\frac{1}{\Delta} [q_1 \Delta_1 \exp(-q_1 y) + q_2 \Delta_2 \exp(-q_2 y) - \mathrm{i}\xi \{\Delta_3 \exp(-q_3 y) + \Delta_4 \exp(-q_4 y)\}], \tag{32}$$

$$\tilde{\phi}_3 = \frac{1}{\Delta} [a_3^* \Delta_3 \exp(-q_3 y) + a_4^* \Delta_4 \exp(-q_4 y)], \tag{33}$$

$$\tilde{t}_{22} = \frac{1}{\Delta} [r_1 \Delta_1 \exp(-q_1 y) + r_2 \Delta_2 \exp(-q_2 y) + r_3 \Delta_3 \exp(-q_3 y) + r_4 \Delta_4 \exp(-q_4 y)], \tag{34}$$

$$\tilde{t}_{21} = \frac{1}{\Delta} [s_1 \Delta_1 \exp(-q_1 y) + s_2 \Delta_2 \exp(-q_2 y) + s_3 \Delta_3 \exp(-q_3 y) + s_4 \Delta_4 \exp(-q_4 y)], \tag{35}$$

$$\tilde{m}_{23} = -\frac{B_3 \omega^2}{\rho c_1^4 \Delta} [a_3^* q_3 \Delta_3 \exp(-q_3 y) + a_4^* q_4 \Delta_4 \exp(-q_4 y)], \tag{36}$$

$$\widetilde{T} = \frac{1}{\Delta} [a_1^* \Delta_1 \exp(-q_1 y) + a_2^* \Delta_2 \exp(-q_2 y)], \tag{37}$$

where

$$\begin{aligned}
&\Delta = f_1 f_2 - f_3 f_4, \qquad f_1 = s_1 g_2^* - s_2 g_1^*, \qquad f_2 = a_3^* q_3 r_4 - a_4^* q_4 r_3, \\
&f_3 = r_1 g_2^* - r_2 g_1^*, \qquad f_4 = a_3^* q_3 s_4 - a_4^* q_4 s_3, \\
&\Delta_{1,2} = \pm F f_4 g_{2,1}^* \tilde{\Psi}_1(\xi), \qquad \Delta_{3,4}^* = \pm F a_{4,3}^* q_{4,3} f_1 \tilde{\Psi}_1(\xi), \\
&g_{1,2}^* = a_{1,2}^* (q_{1,2} - h), \qquad r_n = -\xi^2 \frac{A_2}{\rho c_1^2} + q_n^2 - (1 + t_1 \delta_{2k} p) a_n^*, \\
&r_\Theta = -\mathrm{i}\xi q_\Theta \left(1 - \frac{A_2}{\rho c_1^2}\right), \qquad s_n = \mathrm{i}\xi q_n \frac{(A_3 + A_4)}{\rho c_1^2}, \qquad s_\Theta = \frac{1}{\rho c_1^2} [A_3 q_\Theta^2 + \xi^2 A_4 + (A_3 - A_4) a_\Theta^*], \\
&n = 1, 2, \quad \Theta = 3, 4.
\end{aligned} \tag{38}$$

3.1.1. Concentrated force

To determine displacements, microrotation, stresses, and temperature due to a concentrated force described by the Dirac delta function, $\tilde{\Psi}_1(\xi) = \delta(x)$ must be used with

$$\tilde{\Psi}_1(\xi) = 1. \tag{39}$$

3.1.2. Uniformly distributed force

The solution due to uniformly distributed force applied on the half-space is obtained by setting

$$\Psi_1(x) = \begin{bmatrix} 1 & \text{if } |x| \leqslant a, \\ 0 & \text{if } |x| > a \end{bmatrix}$$

in Eqs. (30). The Fourier transform, with respect to the pair (x, ξ) for the case of a uniform strip load of unit amplitude and width $2a$ applied at the origin of the coordinate system ($x = y = 0$) in dimensionless form after suppressing the primes, becomes

$$\tilde{\Psi}_1(\xi) = \left[2\sin\left(\frac{\xi c_1 a}{\omega}\right)\Big/\xi\right], \quad \xi \neq 0. \tag{40}$$

3.1.3. Linearly distributed force

The solution due to a linearly distributed force is obtained by substituting

$$\Psi_1(x) = \begin{bmatrix} 1 - \frac{|x|}{a} & \text{if } |x| \leqslant a, \\ 0 & \text{if } |x| > a, \end{bmatrix}$$

in Eqs. (30), where $2a$ is the width of the strip load. The Fourier transform in the case of a linearly distributed force applied at the origin on the system in dimensionless form is

$$\tilde{\Psi}_1(\xi) = \frac{2[1 - \cos(\xi c_1 a/\omega)]}{\xi^2 c_1 a/\omega}. \tag{41}$$

The expressions for displacements, stresses, and temperature can be obtained for a concentrated, uniformly and linearly distributed force by replacing $\tilde{\Psi}_1(\xi)$ from (39)–(41), respectively, in (31)–(37).

3.2. Thermoelastic interactions due to a thermal source

The boundary conditions in this case are

$$\begin{aligned} &t_{22} = 0, \quad t_{21} = 0, \quad m_{23} = 0, \quad \frac{\partial T}{\partial y} = \eta(x)\delta(t), \text{ for temperature gradient boundary} \\ &\text{or} \\ &T(x, y = 0) = r(x, t), \text{ for temperature input boundary,} \end{aligned} \tag{42}$$

where $r(x, t) = \eta(x)\delta(t)$.

Applying Laplace and Fourier transforms defined by (19) and (20), we get

$$r(\xi, p) = \tilde{\eta}(\xi).$$

The expressions for displacement, force stress, tangential couple stress, and temperature distribution are given by Eqs. (31)–(37) with Δ_υ replaced by Δ^0_υ ($\upsilon = 1, 2, 3, 4$) in Eqs. (38), where

$$\begin{aligned} \Delta^0_{1,2} &= \mp H\tilde{\eta}(\xi)[-a^*_3 q_3(r_{2,1}s_4 - r_4 s_{2,1}) + a^*_4 q_4(r_{2,1}s_3 - r_3 s_{2,1})], \\ \Delta^0_{3,4} &= \mp H\tilde{\eta}(\xi) a^*_{4,3} q_{4,3}(r_1 s_2 - r_2 s_1), \end{aligned} \tag{43}$$

where $H = -\frac{c_1}{\omega T_0}$ for temperature gradient boundary and $H = \frac{1}{T_0}$ for temperature input boundary.

3.2.1. Thermal source

In this case

$$\eta(x) = \delta(x)$$

with

$$\tilde{\eta}(\xi) = 1. \tag{44}$$

3.2.2. Uniformly distributed thermal source

In this case

$$\eta(x) = \begin{cases} 1 & \text{if } |x| \leqslant a, \\ 0 & \text{if } |x| > a, \end{cases}$$

with

$$\tilde{\eta}(\xi) = \left[2\sin\left(\frac{\xi c_1 a}{\omega}\right)\Big/\xi\right], \quad \xi \neq 0. \tag{45}$$

3.2.3. Linearly distributed thermal source

In this case

$$\eta(x) = \begin{cases} 1 - \dfrac{|x|}{a} & \text{if } |x| \leqslant a, \\ 0 & \text{if } |x| > a, \end{cases}$$

with

$$\tilde{\eta}(\xi) = \frac{2[1-\cos(\xi c_1 a/\omega)]}{\xi^2 c_1 a/\omega}. \tag{46}$$

The expressions for displacements, microrotation, stresses, and temperature can be obtained for a thermal point source and for uniformly and linearly distributed thermal sources by replacing $\tilde{\eta}(\xi)$ from (44)–(46), respectively, in (31)–(37).

4. Particular cases

4.1. Neglecting micropolarity effects (i.e., $B_3 = j = 0$), we obtain the corresponding expressions for displacements, stresses, and temperature distribution as

$$\tilde{u}_1 = -\frac{1}{\Delta^*}[\mathrm{i}\xi\{\Delta_1^* \exp(-q_1 y) + \Delta_2^* \exp(-q_2 y)\} + q_3 \Delta_3^* \exp(-q_3' y)], \tag{47}$$

$$\tilde{u}_2 = -\frac{1}{\Delta^*}[q_1 \Delta_1^* \exp(-q_1 y) + q_2 \Delta_2^* \exp(-q_2 y) - \mathrm{i}\xi \Delta_3^* \exp(-q_3' y)], \tag{48}$$

$$\tilde{t}_{22} = \frac{1}{\Delta^*}[r_1 \Delta_1^* \exp(-q_1 y) + r_2 \Delta_2^* \exp(-q_2 y) + r_3^* \Delta_3^* \exp(-q_3' y)], \tag{49}$$

$$\tilde{t}_{21} = \frac{1}{\Delta^*}[s_1 \Delta_1^* \exp(-q_1 y) + s_2 \Delta_2^* \exp(-q_2 y) + s_3^* \Delta_3^* \exp(-q_3' y)], \tag{50}$$

$$\tilde{T} = \frac{1}{\Delta^*}[a_1^* \Delta_1^* \exp(-q_1 y) + a_2^* \Delta_2^* \exp(-q_2 y)], \tag{51}$$

where

$$\begin{aligned} &\Delta^* = g_1^*(r_2 s_3^* - r_3^* s_2) - g_2^*(r_1 s_3^* - r_3^* s_1), \qquad \Delta_{1,2}^* = \pm F\tilde{\Psi}_1(\xi) g_{2,1}^* s_3^*, \\ &\Delta_3^* = -F\tilde{\Psi}_1(\xi)(s_1 g_2^* - s_2 g_1^*), \qquad r_3^* = -\mathrm{i}\xi q_3'\left(1 - \frac{A_2}{\rho c_1^2}\right), \\ &s_3^* = \frac{1}{\rho c_1^2}(A_3 q_3'^2 + \xi^2 A_4), \qquad q_3'^2 = \frac{a_{12}\xi^2 + p^2}{a_{13}}. \end{aligned} \tag{52}$$

4.1.1. The expressions for displacements, stresses, and temperature can be obtained for a concentrated, uniformly and linearly distributed force by replacing $\tilde{\Psi}_1(\xi)$ from (39)–(41) respectively in (47)–(51).

4.1.2. The expressions for displacement, force stress, and temperature distribution for thermal sources are given by Eqs. (47)–(51) with Δ^*_Ξ replaced by Δ^{*0}_Ξ ($\Xi = 1,2,3$) in Eq. (52), where

$$\Delta^{*0}_1 = H\tilde{\eta}(\xi)(r_2 s^*_3 - r^*_3 s_2), \qquad \Delta^{*0}_2 = -H\tilde{\eta}(\xi)(r_1 s^*_3 - r^*_3 s_1), \qquad \Delta^{*0}_3 = H\tilde{\eta}(\xi)(r_1 s_2 - r_2 s_1). \tag{53}$$

The expressions for displacements, stresses, and temperature distribution can be obtained for a thermal point source and for uniformly and linearly distributed thermal sources by replacing $\tilde{\eta}(\xi)$ from (44)–(46), respectively, in (47)–(51) and using (53).

4.2. Neglecting thermal effects the expressions for displacements, microrotation, and stresses are obtained as

$$\tilde{u}_1 = -\frac{1}{\Delta^{**}}[\mathrm{i}\xi\Delta^{**}_1 \exp(-q'_1 y) + q_3\Delta^{**}_3 \exp(-q_3 y) + q_4\Delta^{**}_4 \exp(-q_4 y)], \tag{54}$$

$$\tilde{u}_2 = -\frac{1}{\Delta^{**}}[q'_1\Delta^{**}_1 \exp(-q'_1 y) - \mathrm{i}\xi\{\Delta^{**}_3 \exp(-q_3 y) + \Delta^{**}_4 \exp(-q_4 y)\}], \tag{55}$$

$$\tilde{\phi}_3 = \frac{1}{\Delta^{**}}[a^*_3\Delta^{**}_3 \exp(-q_3 y) + a^*_4\Delta^{**}_4 \exp(-q_4 y)], \tag{56}$$

$$\tilde{t}_{22} = \frac{1}{\Delta^{**}}[r^*_1\Delta^{**}_1 \exp(-q'_1 y) + r_3\Delta^{**}_3 \exp(-q_3 y) + r_4\Delta^{**}_4 \exp(-q_4 y)], \tag{57}$$

$$\tilde{t}_{21} = \frac{1}{\Delta^{**}}[s^*_1\Delta^{**}_1 \exp(-q'_1 y) + s_3\Delta^{**}_3 \exp(-q_3 y) + s_4\Delta^{**}_4 \exp(-q_4 y)], \tag{58}$$

$$\tilde{m}_{23} = -\frac{B_3\omega^2}{\rho c_1^4\Delta^{**}}[a^*_3 q_3\Delta^{**}_3 \exp(-q_3 y) + a^*_4 q_4\Delta^{**}_4 \exp(-q_4 y)], \tag{59}$$

where

$$\begin{aligned}
&\Delta^{**} = -a^*_3 q_3(r^*_1 s_4 - r_4 s^*_1) + a^*_4 q_4(r^*_1 s_3 - r_3 s^*_1),\\
&\Delta^{**}_1 = -F\tilde{\Psi}_1(\xi)(a^*_4 q_4 s_3 - a^*_3 q_3 s_4), \qquad \Delta^{**}_{2,3} = \pm F\tilde{\Psi}_1(\xi) s^*_1 a^*_{4,3} q_{4,3},\\
&s^*_1 = \mathrm{i}\xi q'_1\frac{(A_3 + A_4)}{\rho c_1^2}, \qquad r^*_1 = -\frac{\xi^2 A_2}{\rho c_1^2} + q'^2_1, \qquad q'^2_1 = \frac{\xi^2 + p^2}{a_{11}}.
\end{aligned} \tag{60}$$

Again the expressions for displacements, microrotation, force stress and couple stress can be obtained for a concentrated, uniformly and linearly distributed force by replacing $\tilde{\Psi}(\xi)$ from (39)–(41), respectively, in (54)–(59).

4.2.1. Sub case 1. If $h \to 0$, (31)–(37) and (47)–(51) yield the expressions for displacements, microrotation, stresses, and temperature distribution for an insulated boundary. In this case $H = -c_1/\omega T_0$ in Eq. (43).

4.2.2. Sub case 1. If $h \to \infty$, (31)–(37) and (47)–(51) yield the expressions for displacements, microrotation, stresses, and temperature distribution for an isothermal boundary. In this case $H = 1/T_0$ in Eq. (43).

4.2.3. Special case 1. By putting $k = 1$ and $t_1 = 0$ in (31)–(37) and (47)–(51), we obtain the displacements, microrotation, stresses, and temperature distribution for L–S theory (Lord and Shulman, 1967).

4.2.4. Special case 2. For G–L theory (Green and Lindsay, 1972), we obtain the corresponding expressions for displacements, microrotation, stresses, and temperature distribution by substituting $k = 2$ into (31)–(37) and (47)–(51).

4.3. Micropolar thermoelastic solid

4.3.1. Taking

$$A_1 = \lambda + 2\mu + K, \qquad A_2 = \lambda, \qquad A_3 = \mu + K, \qquad A_4 = \mu, \qquad B_3 = \gamma \tag{61}$$

in Eqs. (31)–(37), (47)–(51) and (54)–(59) with (39)–(41) we obtain the corresponding expressions in a micropolar thermoelastic isotropic medium, thermoelastic isotropic medium, and micropolar isotropic medium for concentrated, uniformly distributed, and linearly distributed force, respectively.

4.3.2. Using Eqs. (61) in Eqs. (31)–(37) with Δ_υ replaced by Δ_υ^0 ($\upsilon = 1,2,3,4$) from Eq. (43) and using Eqs. (44)–(46) we obtain the corresponding expressions for thermal source, uniformly thermal source, and linearly distributed thermal source, respectively.

5. Inversion of the transformed

The transformed displacements and stresses are functions of y, the parameters of Laplace and Fourier transforms p and ξ, respectively, and hence are of the form $\tilde{f}(\xi, y, p)$. To get the function in the physical domain, first we invert the Fourier transform using

$$\bar{f}(x,y,p) = \frac{1}{2\pi}\int_{-\infty}^{\infty} \mathrm{e}^{-\mathrm{i}\xi x}\tilde{f}(\xi,y,p)\,\mathrm{d}\xi = \frac{1}{\pi}\int_0^{\infty}\{\cos(\xi x)f_{\mathrm{e}} - \mathrm{i}\sin(\xi x)f_{\mathrm{o}}\}\,\mathrm{d}\xi, \tag{62}$$

where f_{e} and f_{o}, are even and odd parts of the function $\tilde{f}(\xi, y, p)$, respectively. Thus, expressions (62) give us the transform $\bar{f}(x, y, p)$ of the function $f(x, y, t)$. Now, for the fixed values of ξ, x, and y, the $\bar{f}(x, y, p)$ in the expression (40) can be considered as the Laplace transform $\bar{g}(p)$ of some function $g(t)$. Following Honig and Hirdes (1984), the Laplace transformed function $\bar{g}(p)$ can be converted as given below.

The function $g(t)$ can be obtained by using

$$g(t) = \frac{1}{2\pi\mathrm{i}}\int_{c-\mathrm{i}\infty}^{c+\mathrm{i}\infty} \mathrm{e}^{pt}\bar{g}(p)\,\mathrm{d}p, \tag{63}$$

where C is an arbitrary real number greater than all the real parts of the singularities of $\bar{g}(p)$. Taking $p = C + \mathrm{i}y$, we get

$$g(t) = \frac{\mathrm{e}^{Ct}}{2\pi}\int_{-\infty}^{\infty} \mathrm{e}^{\mathrm{i}ty}\bar{g}(C+\mathrm{i}y)\,\mathrm{d}y. \tag{64}$$

Now, taking $\mathrm{e}^{-Ct}g(t)$ as $h(t)$ and expanding it as Fourier series in $[0, 2L]$, we obtain the approximate formula

$$g(t) = g_\infty(t) + E_{\mathrm{D}},$$

where

$$g_\infty(t) = \frac{C_0}{2} + \sum_{k=1}^{\infty} C_k, \quad 0 \leqslant t \leqslant 2L,$$

$$C_k = \frac{\mathrm{e}^{ct}}{L}\Re\left[\mathrm{e}^{\frac{\mathrm{i}k\pi t}{L}}\bar{g}\left(C + \frac{\mathrm{i}k\pi}{L}\right)\right], \tag{65}$$

and E_{D} is the discretization error and can be made arbitrary small by choosing C large enough. The value of C and L are chosen according to the criteria outlined by Honig and Hirdes (1984).

Since the infinite series in Eq. (65) can be summed up only to a finite number of N terms, the approximate value of $g(t)$ becomes

$$g_N(t) = \frac{C_0}{2} + \sum_{k=1}^{N} C_k, \quad 0 \leqslant t \leqslant 2L. \tag{66}$$

Now, we introduce a truncation error E_I that must be added to the discretization error to produce the total approximation error in evaluating $g(t)$ using the above formula. Two methods are used to reduce the total error. The discretization error is reduced using the "Korrecktur"-method, Honig and Hirdes (1984), and then the "ε-algorithm" is used to reduce the truncation error and hence to accelerate the convergence.

The "Korrecktur"-method formula to evaluate the function $g(t)$ is

$$g(t) = g_\infty(t) - \mathrm{e}^{-2CL}g_\infty(2L+t) + E_{\mathrm{D}'}, \tag{67}$$

where

$$|E_{D'}| \ll |E_D|. \tag{68}$$

Thus, the approximate value of $g(t)$ becomes

$$g_{N_k}(t) = g_N(t) - e^{-2CL} g_{N'}(2L + t), \tag{69}$$

where, N' is an integer such that $N' < N$.

We shall now describe the ε-algorithm that is used to accelerate the convergence of the series in Eq. (66). Let N be a natural number and $S_m = \sum_{k=1}^{m} C_k$ be the sequence of partial sums of Eq. (66). We define the ε-sequence by

$$\varepsilon_{0,m} = 0, \qquad \varepsilon_{1,m} = S_m,$$
$$\varepsilon_{n+1,m} = \varepsilon_{n-1,m+1} + \frac{1}{\varepsilon_{n,m+1} - \varepsilon_{n,m}}; \quad n, m = 1, 2, 3, \ldots.$$

It can be shown (Honig and Hirdes, 1984) that the sequence $\varepsilon_{1,1}, \varepsilon_{3,1}, \ldots, \varepsilon_{N,1}$ converges to $g(t) + E_D - C_0/2$ faster than the sequence of partial S_m, $m = 1, 2, 3 \ldots$. The actual procedure to invert the Laplace transform reduces to the study of Eq. (67) together with the ε-algorithm.

The last step is to evaluate the integral in Eq. (61). The method for evaluating this integral by Press et al. (1986) which involves the use of Rhomberg's integration with adaptive step size. This, also uses the results from successive refinement of the extended trapezoidal rule followed by extrapolation of the results to the limit when the step size tends to zero.

6. Numerical results and discussion

For numerical computations, we take the values of relevant parameters for micropolar cubic crystals as

$$A_1 = 19.6 \times 10^{11} \text{ dyn/cm}^2, \qquad A_3 = 5.6 \times 10^{11} \text{ dyn/cm}^2, \qquad A_2 = 11.7 \times 10^{11} \text{ dyn/cm}^2,$$
$$A_4 = 4.3 \times 10^{11} \text{ dyn/cm}^2, \qquad B_3 = 0.98 \times 10^{-4} \text{ dyn}.$$

For comparison with micropolar isotropic solids, following Eringen (1984) and Dhaliwal and Singh (1980), we take the values of relevant parameters for the case of a magnesium crystal-like material as

$$\rho = 1.74 \text{ gm/cm}^3, \qquad \lambda = 9.4 \times 10^{11} \text{ dyn/cm}^2, \qquad \mu = 4.0 \times 10^{11} \text{ dyn/cm}^2,$$
$$K = 1.0 \times 10^{11} \text{ dyn/cm}^2, \qquad \gamma = 0.779 \times 10^{-4} \text{ dyn}, \qquad j = 0.2 \times 10^{-15} \text{ cm}^2,$$
$$C^* = 0.104 \times 10^7 \text{ cal/gm } ^\circ\text{C}, \qquad v = 0.0268 \times 10^9 \text{ dyn/cm}^2\ ^\circ\text{C}, T_0 = 23\ ^\circ\text{C},$$
$$K^* = 1.7 \text{ J/s cm } ^\circ\text{C}, \qquad t_0 = 6.131 \times 10^{-13} \text{ s}, \qquad t_1 = 8.765 \times 10^{-13} \text{ s}.$$

The values of normal displacement u_2, normal force stress t_{22}, tangential couple stress m_{23}, and temperature distribution T for a micropolar thermoelastic solid with cubic symmetry (MTECC), micropolar thermoelastic isotropic solid (MTEIS), thermoelastic solid with cubic symmetry (TECC), and thermoelastic isotropic solid (TEIS) have been studied for normal force/thermal source and insulated boundary at $t = 0.1$ and $t = 0.25$. The variations of these components with distance x have been shown by (a) solid lines (——) for MTECC and dashed lines (----) for MTEIS for L–S and G–L theories, respectively, (b) solid lines with centered symbols (×—×—×) for MTECC and dashed lines with centered symbols (×---×---×) for MITES for L–S and G–L theories, respectively, (c) solid lines with centered symbols (○—○—○) for TECC and dashed lines with centered symbols (○---○---○) for TEIS for L–S and G–L theories, respectively. These variations are shown in Figs. 1–48. The comparison between micropolar thermoelastic cubic crystal and micropolar thermoelastic isotropic solid is shown. All the results are for one value of dimensionless width $a = 1.0$. The computations are carried out for $y = 1.0$ in the range $0 \leqslant x \leqslant 10.0$.

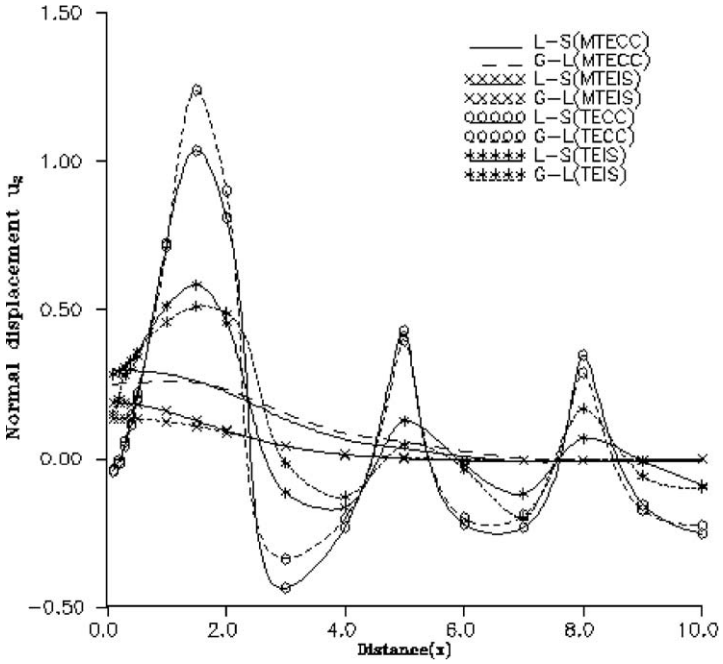

Fig. 1. Variation of normal displacement u_2 with distance x. (Concentrated normal force; insulated boundary.)

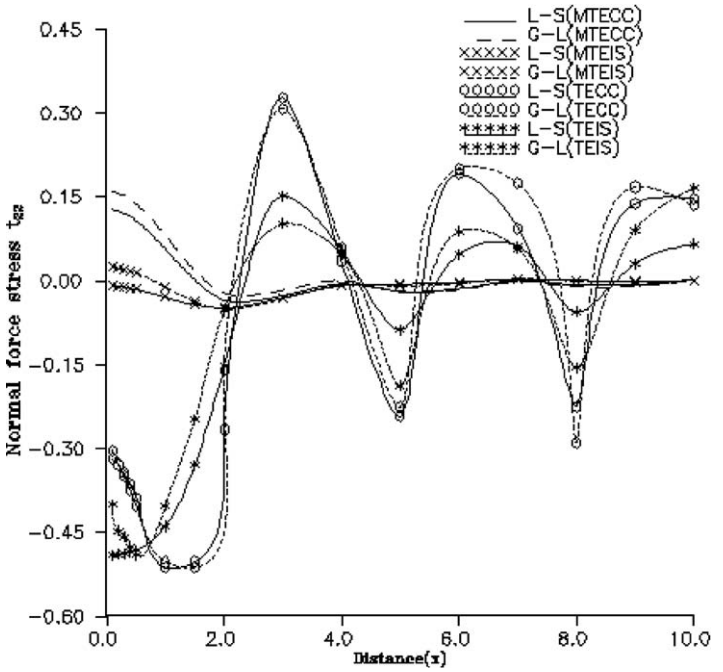

Fig. 2. Variation of normal force stress t_{22} with distance x. (Concentrated normal force; insulated boundary.)

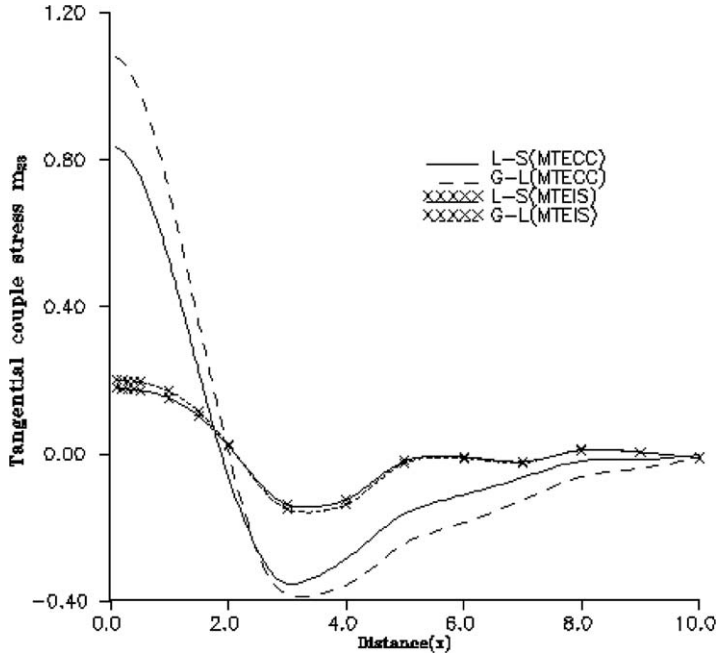

Fig. 3. Variation of tangential couple stress m_{23} with distance x. (Concentrated normal force; insulated boundary.)

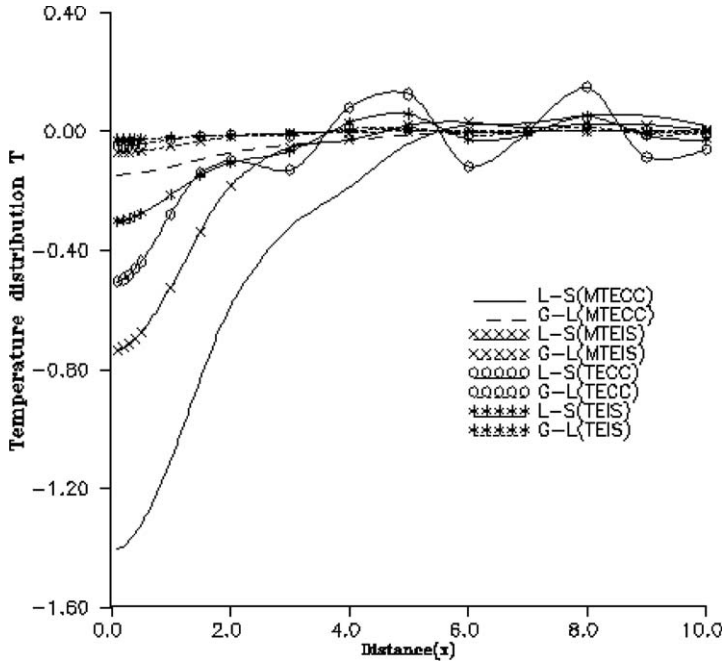

Fig. 4. Variation of temperature distribution T with distance x. (Concentrated normal force; insulated boundary.)

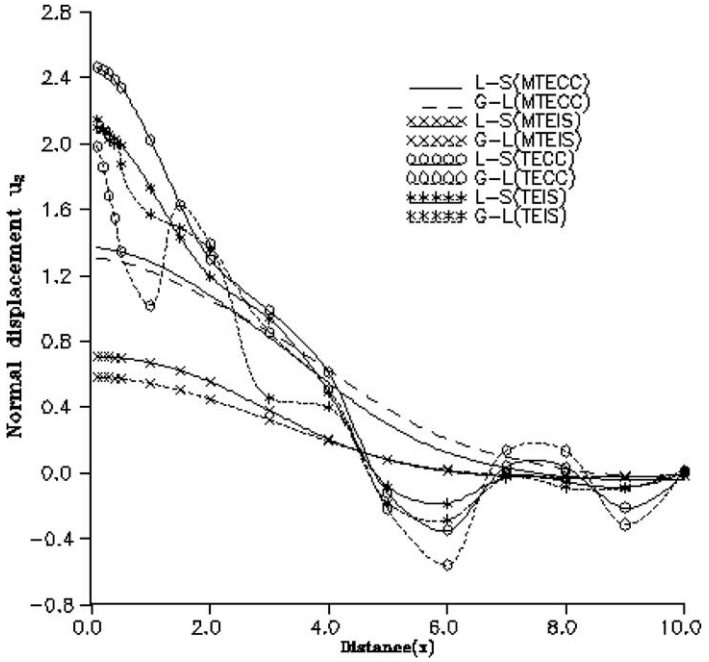

Fig. 5. Variation of normal displacement u_2 with distance x. (Uniformly distributed normal force; insulated boundary.)

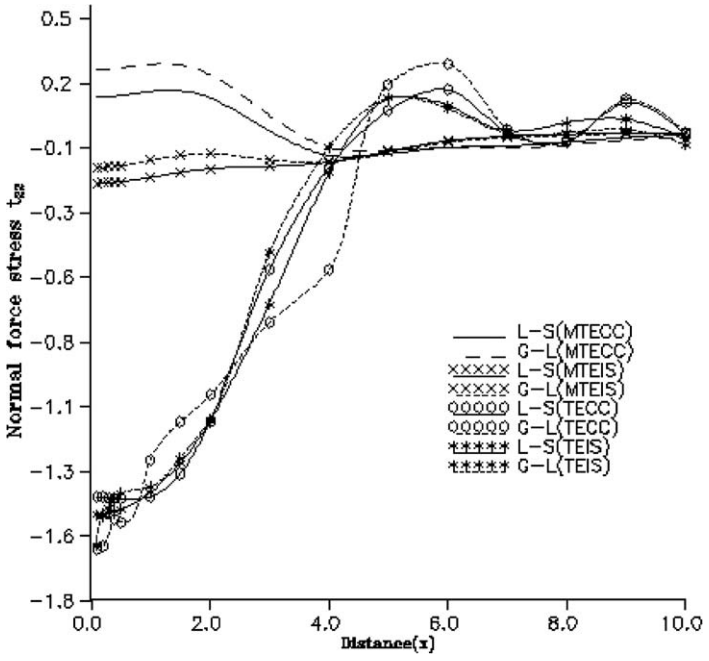

Fig. 6. Variation of normal force stress t_{22} with distance x. (Uniformly distributed normal force; insulated boundary.)

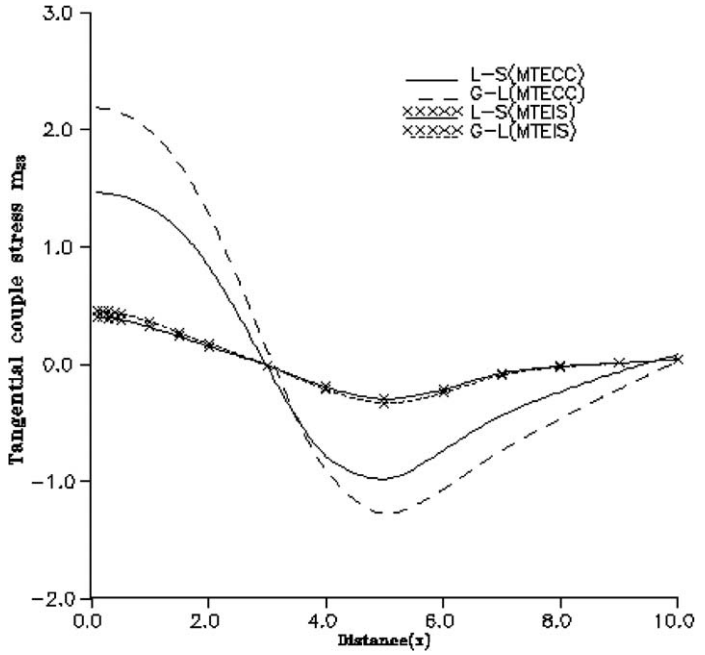

Fig. 7. Variation of tangential couple stress m_{23} with distance x. (Uniformly distributed normal force; insulated boundary.)

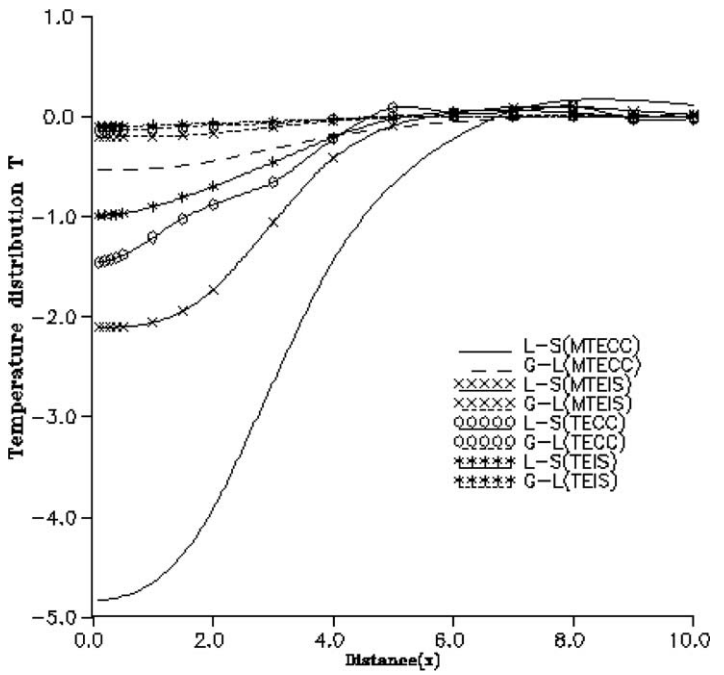

Fig. 8. Variation of temperature distribution T with distance x. (Uniformly distributed normal force; insulated boundary.)

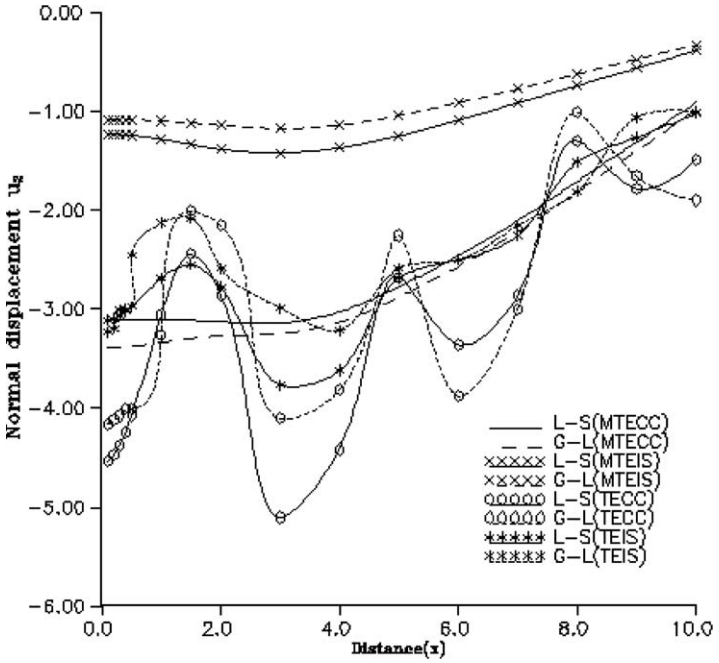

Fig. 9. Variation of normal displacement u_2 with distance x. (Linearly distributed normal force; insulated boundary.)

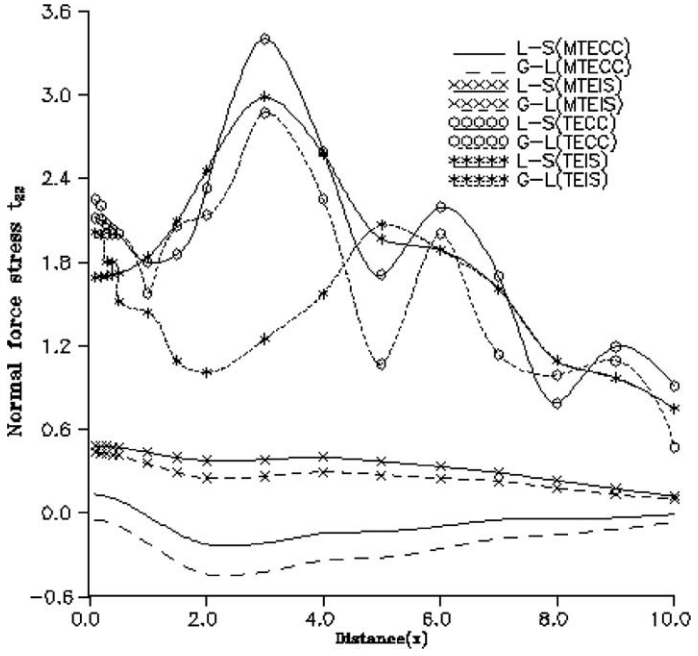

Fig. 10. Variation of normal force stress t_{22} with distance x. (Linearly distributed normal force; insulated boundary.)

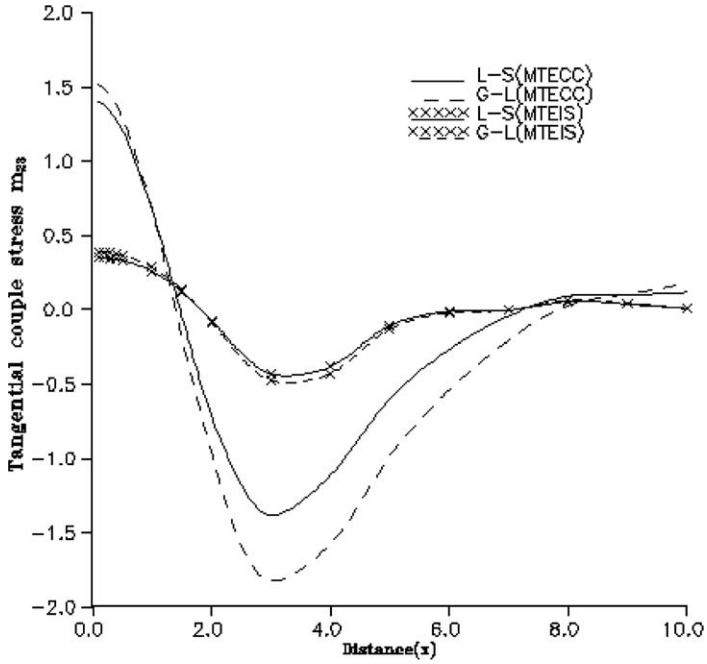

Fig. 11. Variation of tangential couple stress m_{23} with distance x. (Linearly distributed normal force; insulated boundary.)

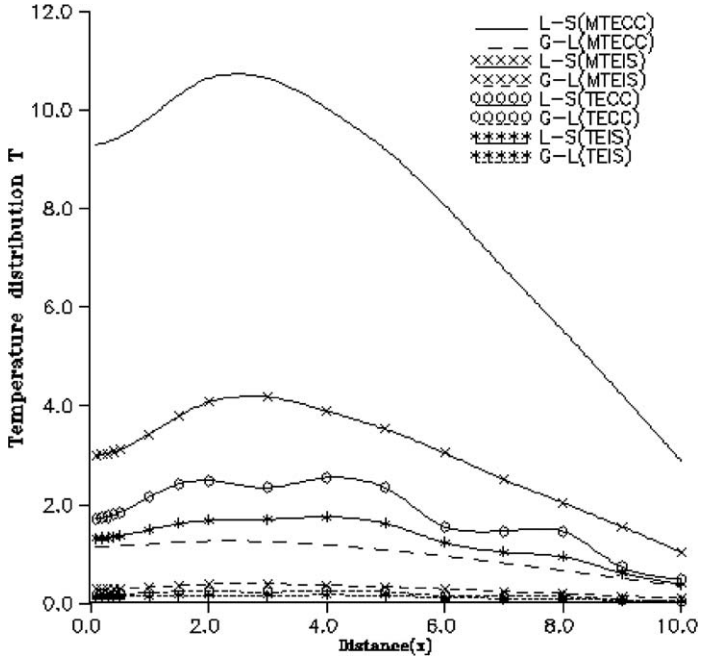

Fig. 12. Variation of temperature distribution T with distance x. (Linearly distributed normal force; insulated boundary.)

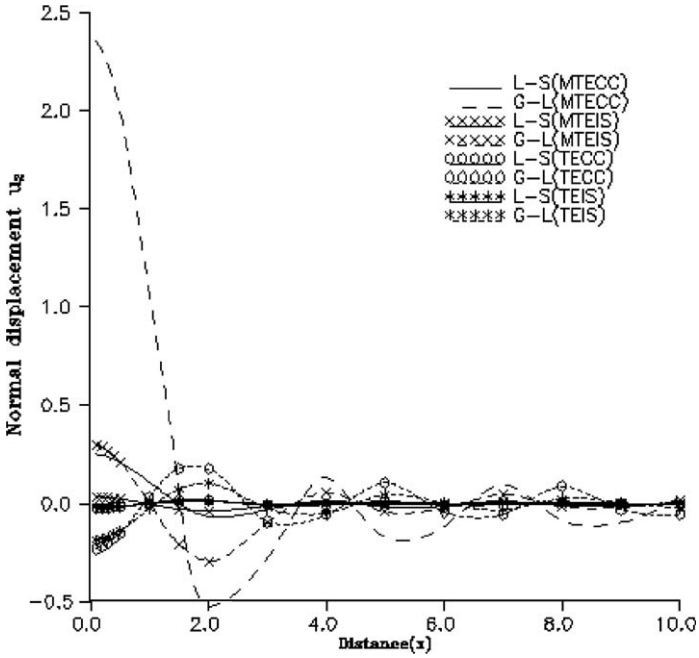

Fig. 13. Variation of normal displacement u_2 with distance x. (Concentrated thermal source; insulated boundary.)

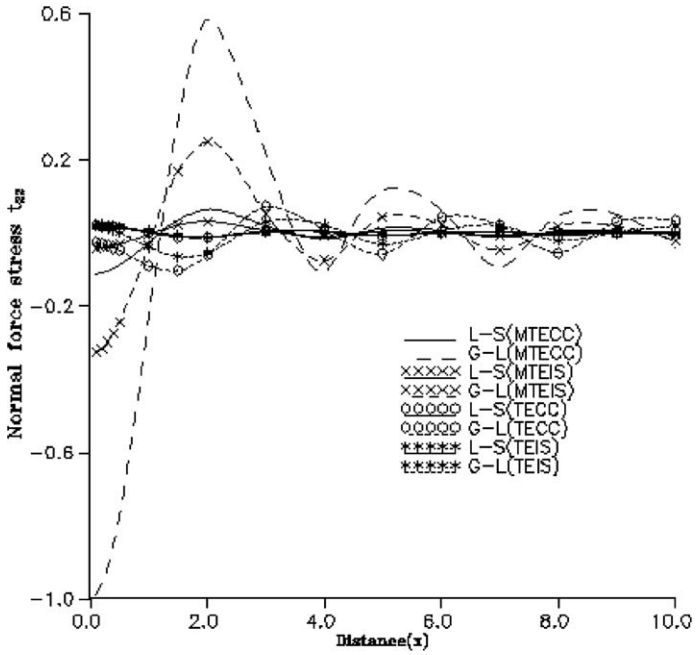

Fig. 14. Variation of normal force stress t_{22} with distance x. (Concentrated thermal source; insulated boundary.)

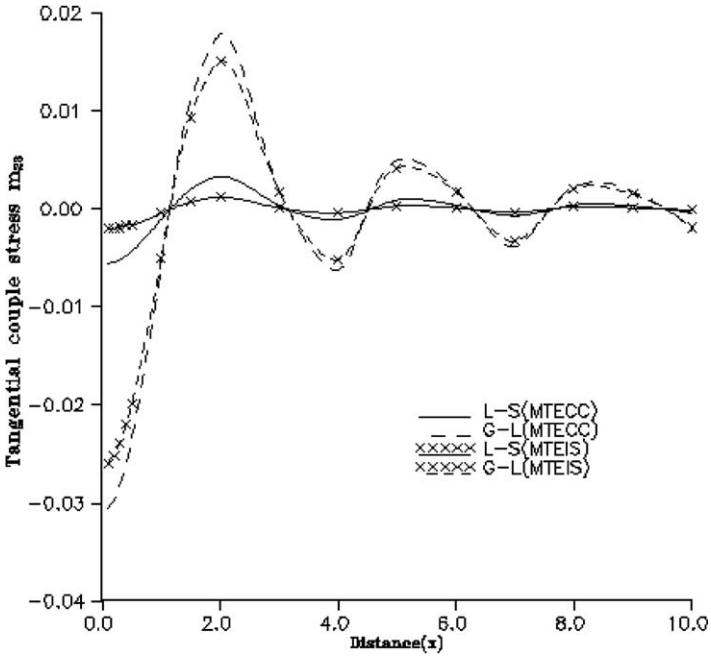

Fig. 15. Variation of tangential couple stress m_{23} with distance x. (Concentrated thermal source; insulated boundary.)

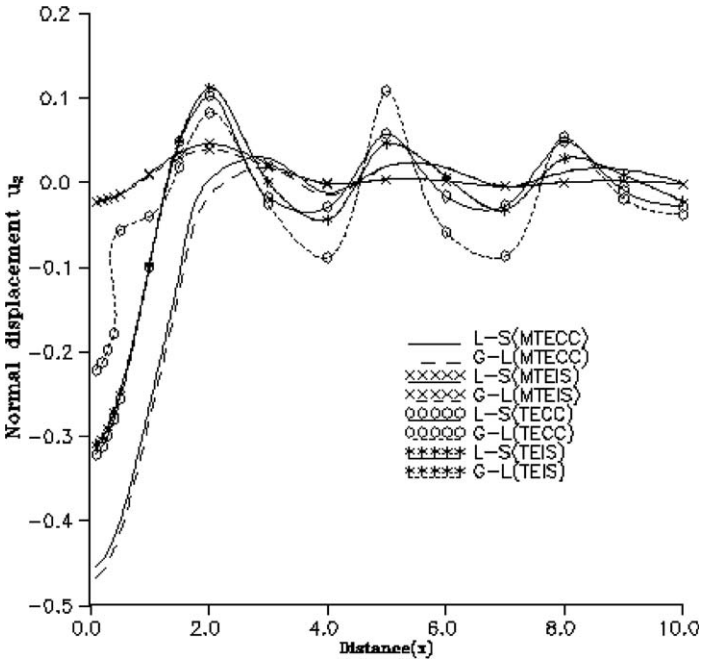

Fig. 16. Variation of temperature distribution T with distance x. (Concentrated thermal source; insulated boundary.)

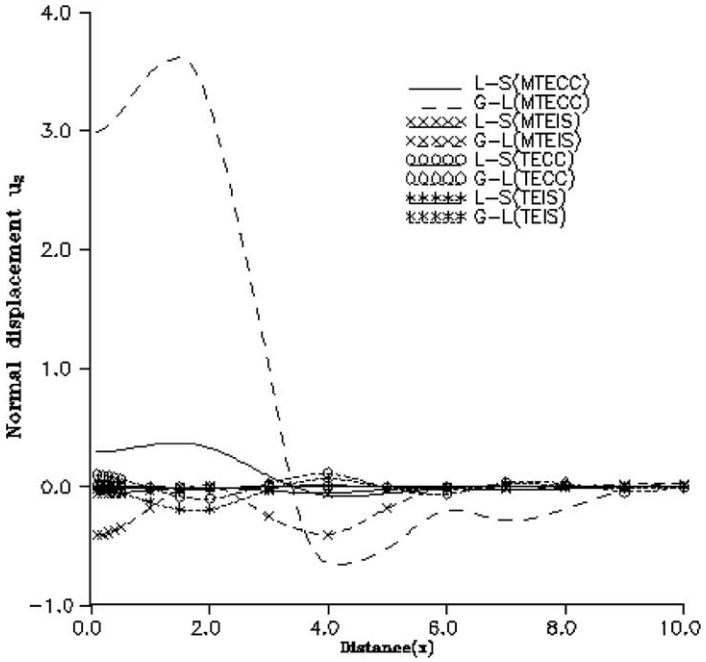

Fig. 17. Variation of normal displacement u_2 with distance x. (Uniformly distributed thermal source; insulated boundary.)

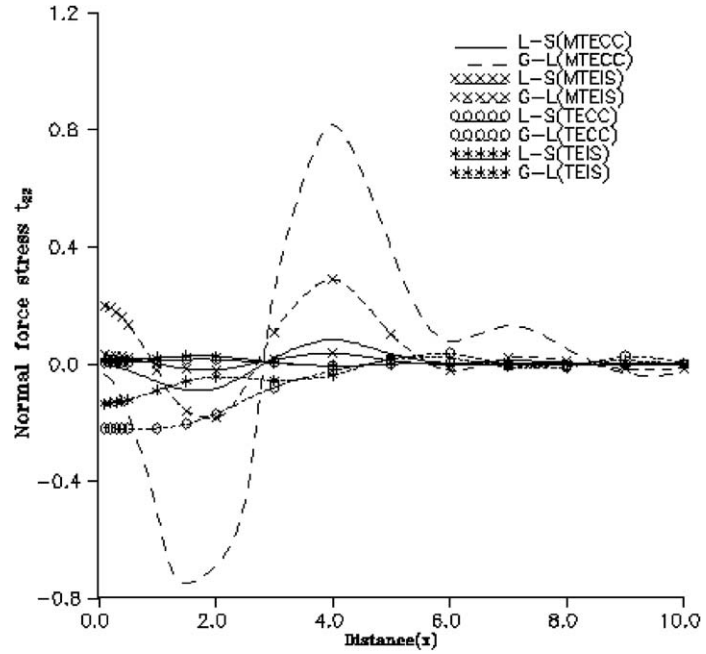

Fig. 18. Variation of normal force stress t_{22} with distance x. (Uniformly distributed thermal source; insulated boundary.)

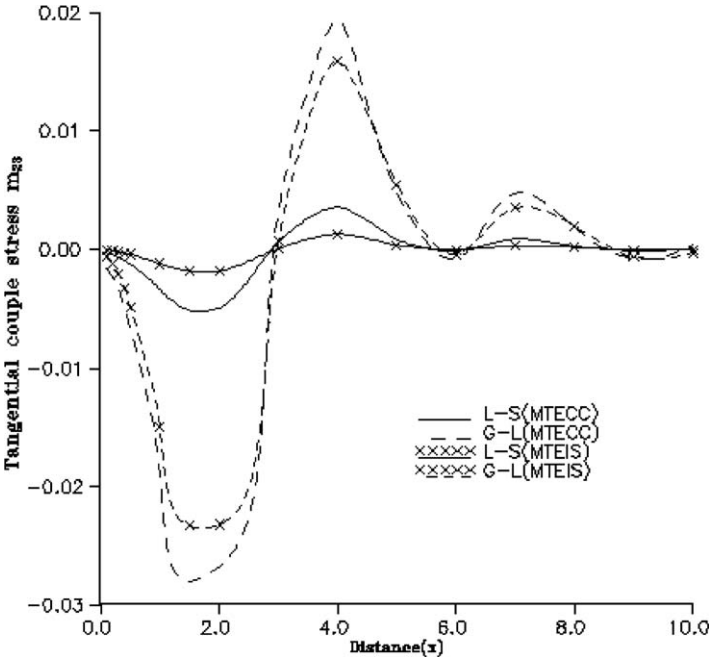

Fig. 19. Variation of tangential couple stress m_{23} with distance x. (Uniformly distributed thermal source; insulated boundary.)

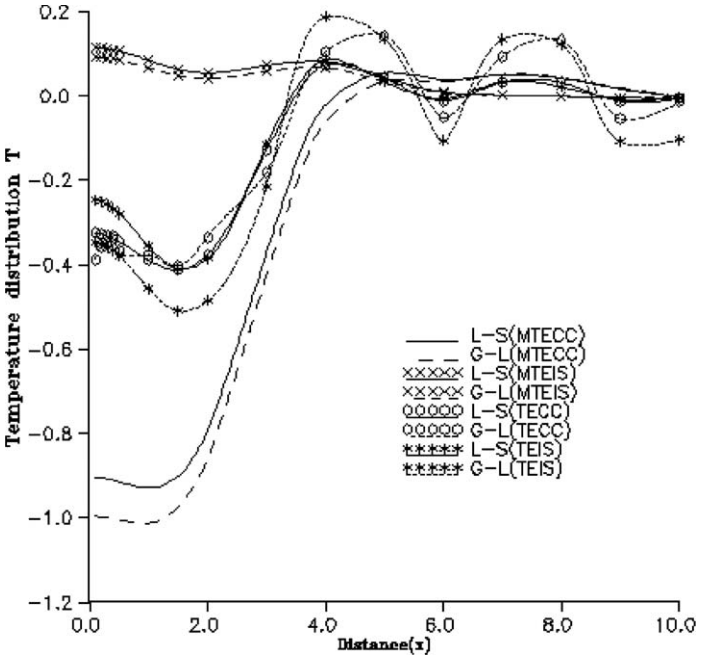

Fig. 20. Variation of temperature distribution T with distance x. (Uniformly distributed thermal source; insulated boundary.)

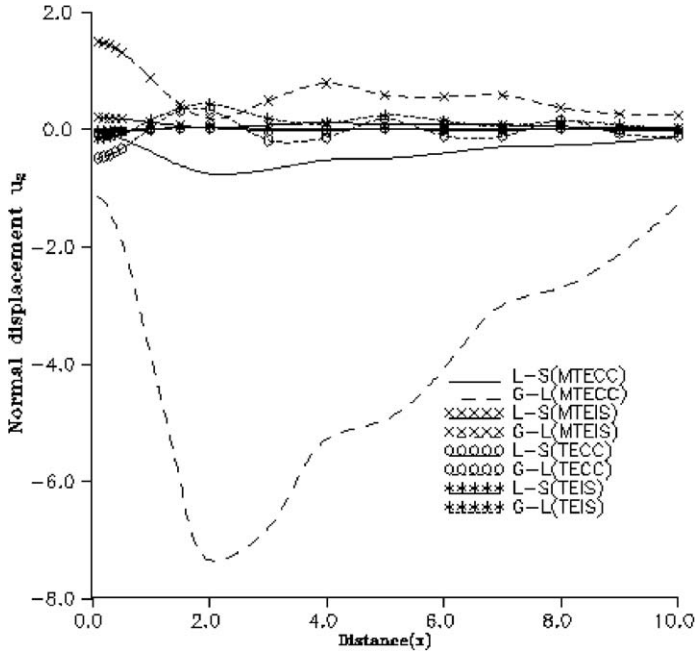

Fig. 21. Variation of normal displacement u_2 with distance x. (Linearly distributed thermal source; insulated boundary.)

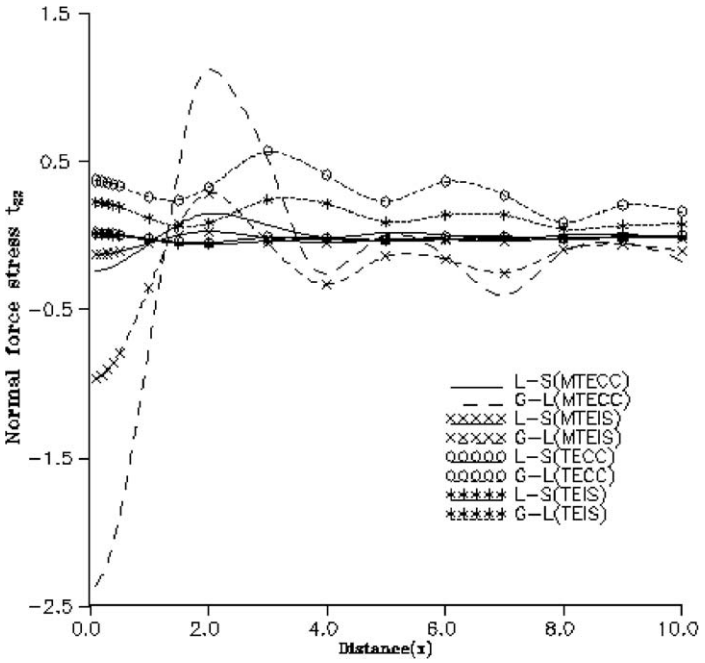

Fig. 22. Variation of normal force stress t_{22} with distance x. (Linearly distributed thermal source; insulated boundary.)

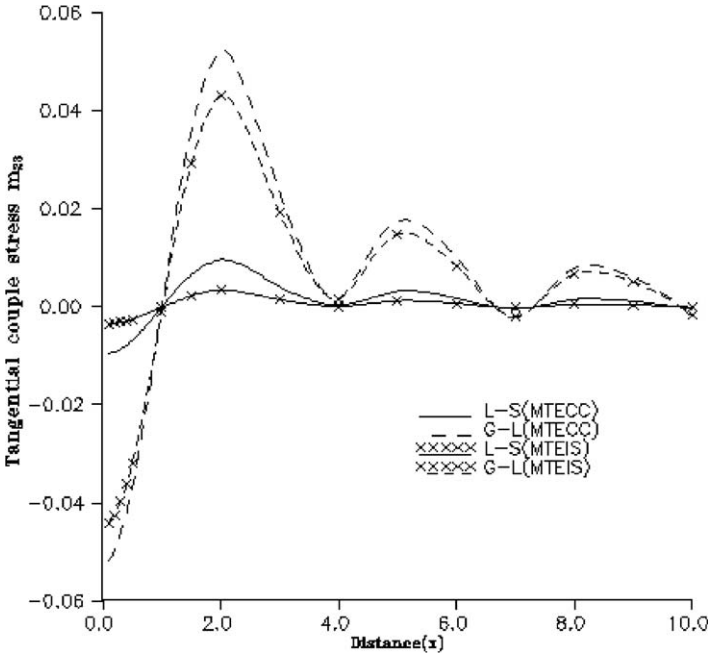

Fig. 23. Variation of tangential couple stress m_{23} with distance x. (Linearly distributed thermal source; insulated boundary.)

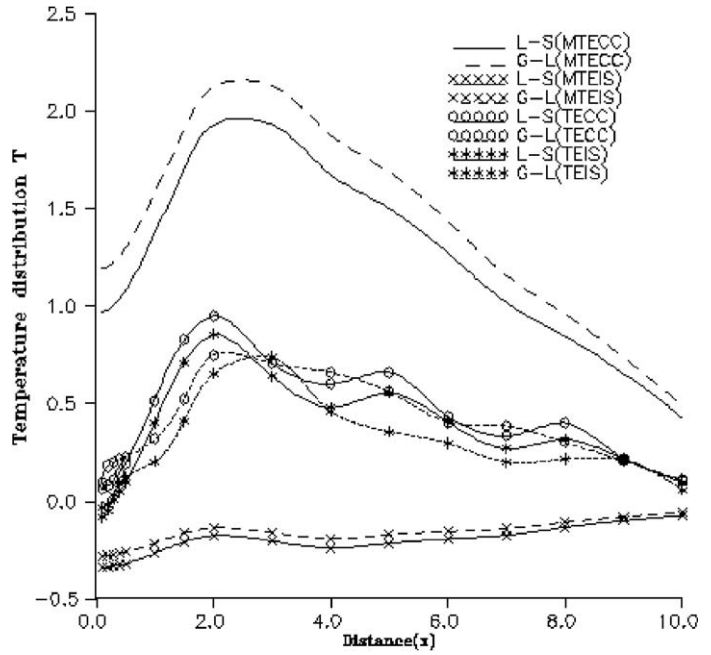

Fig. 24. Variation of temperature distribution T with distance x. (Linearly distributed thermal source; insulated boundary.)

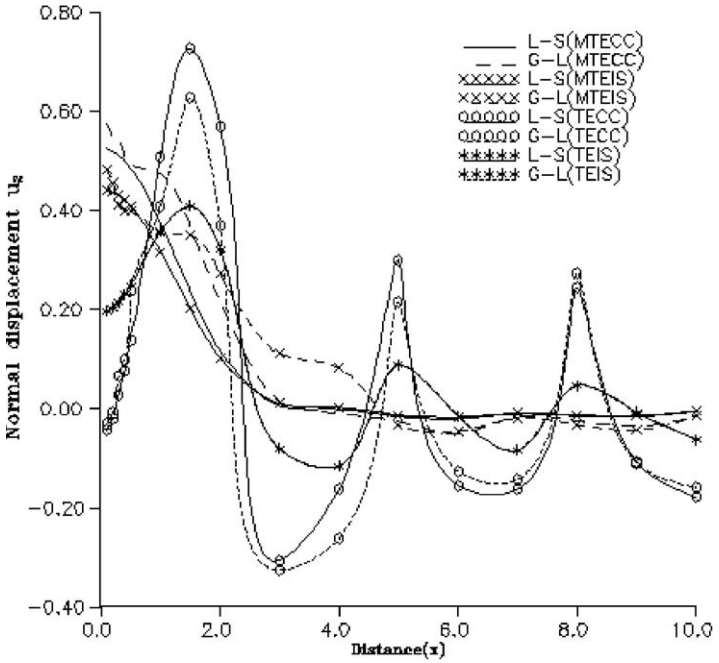

Fig. 25. Variation of normal displacement u_2 with distance x at $t = 0.25$. (Concentrate normal force; insulated boundary.)

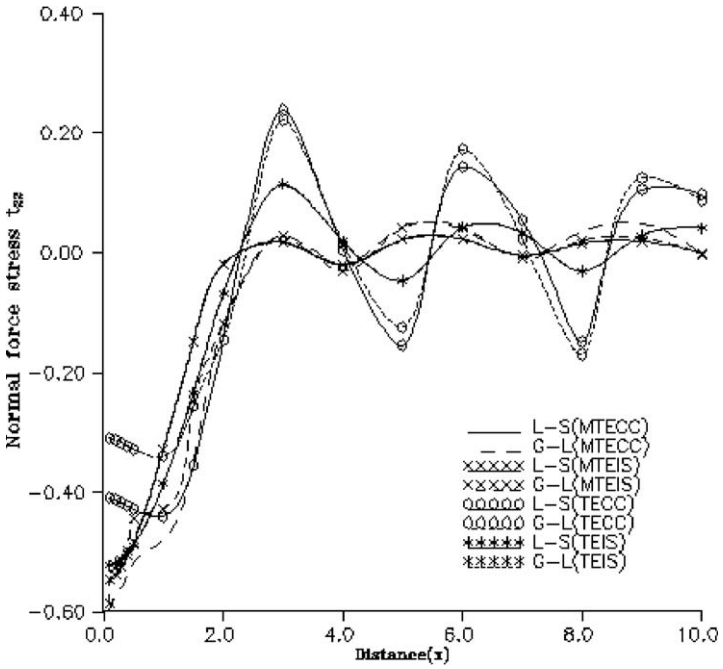

Fig. 26. Variation of normal force stress t_{22} with distance x at $t = 0.25$. (Concentrate normal force; insulated boundary.)

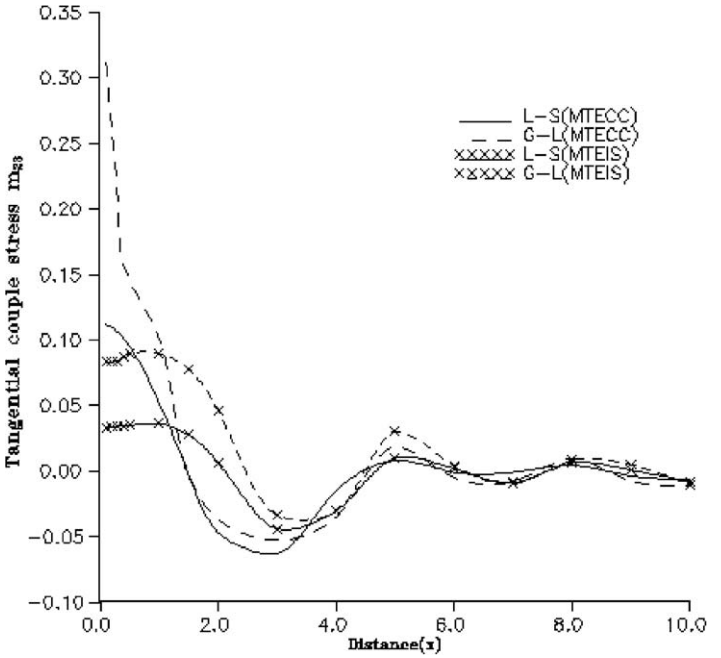

Fig. 27. Variation of tangential couple stress m_{23} with distance x at $t = 0.25$. (Concentrate normal force; insulated boundary.)

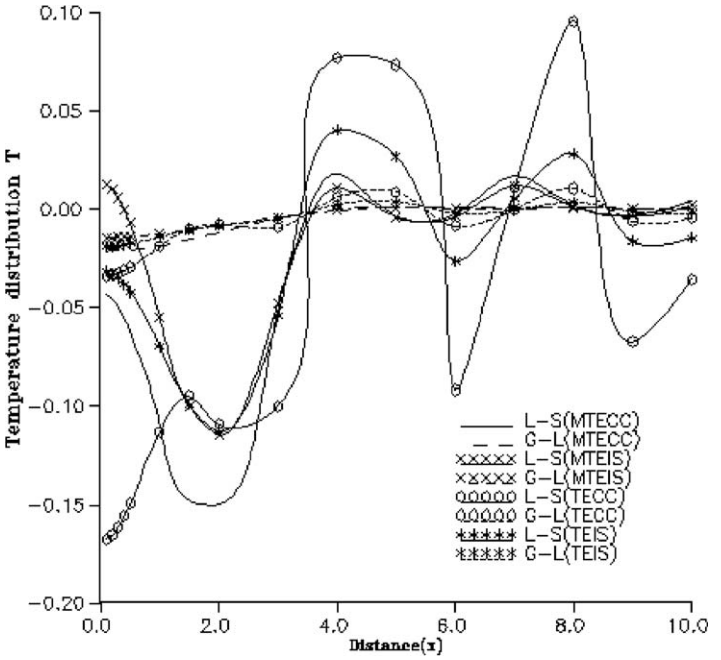

Fig. 28. Variation of temperature distribution T with distance x at $t = 0.25$. (Concentrate normal force; insulated boundary.)

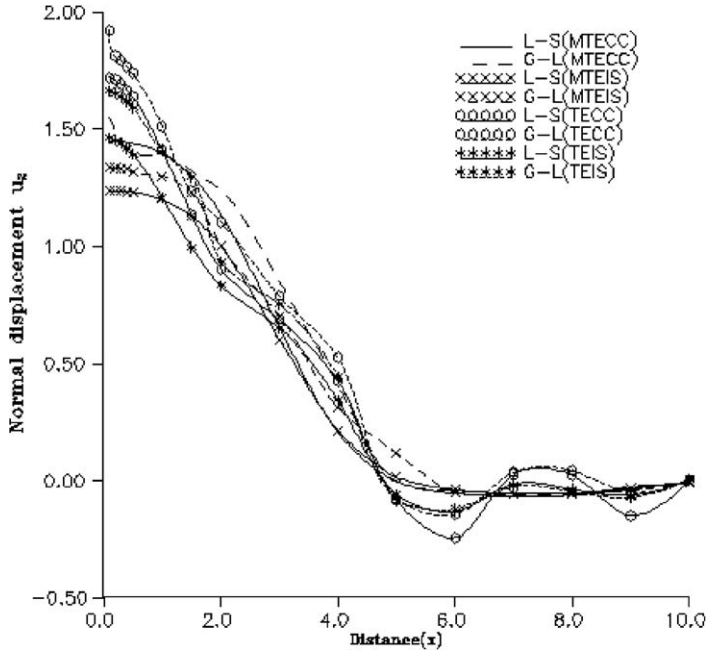

Fig. 29. Variation of normal displacement u_2 with distance x at $t = 0.25$. (Uniformly distributed force; insulated boundary.)

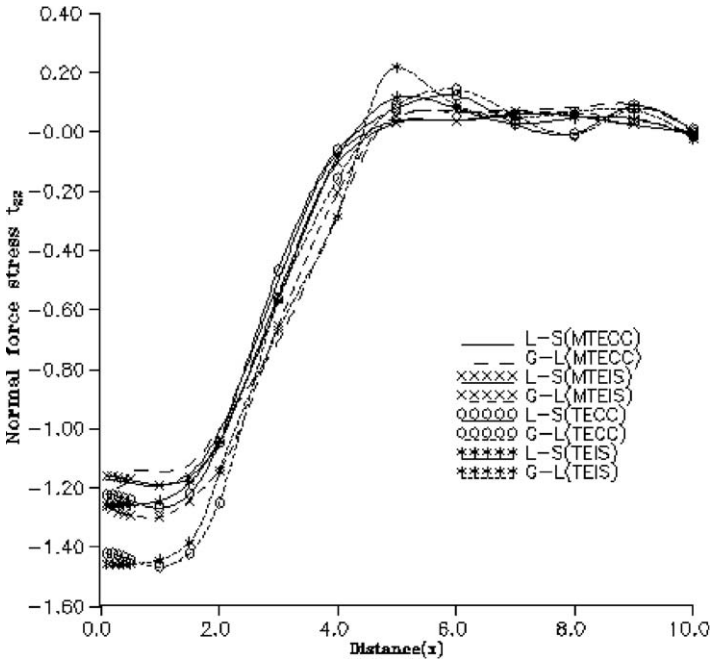

Fig. 30. Variation of normal force stress t_{22} with distance x at $t = 0.25$. (Uniformly distributed force; insulated boundary.)

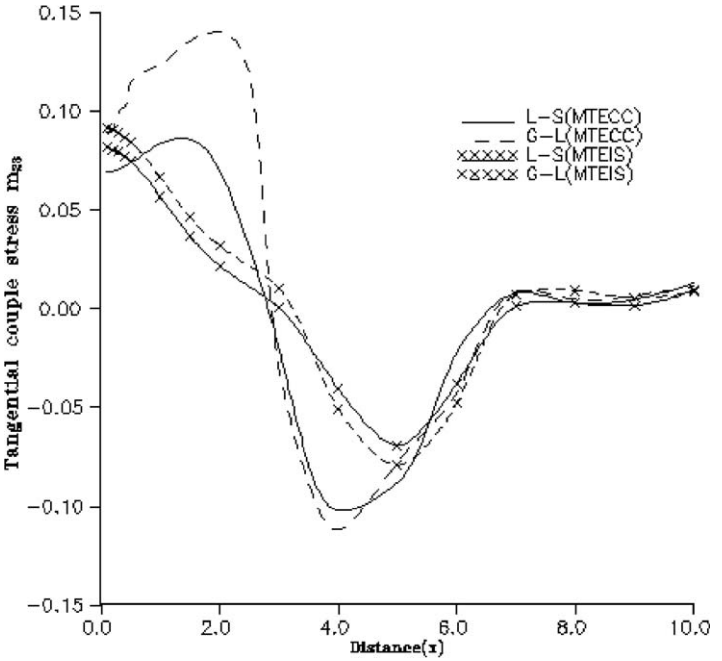

Fig. 31. Variation of tangential couple stress m_{23} with distance x at $t = 0.25$. (Uniformly distributed force; insulated boundary.)

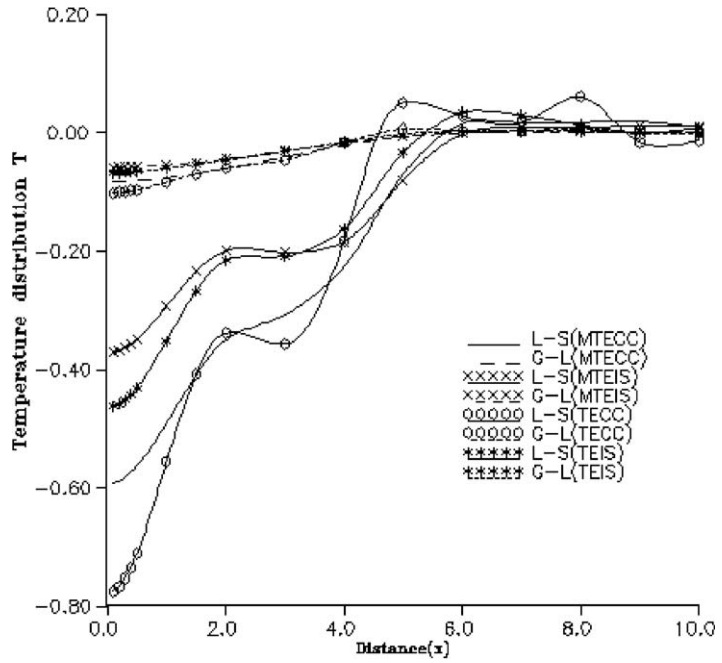

Fig. 32. Variation of temperature distribution T with distance x at $t = 0.25$. (Uniformly distributed force; insulated boundary.)

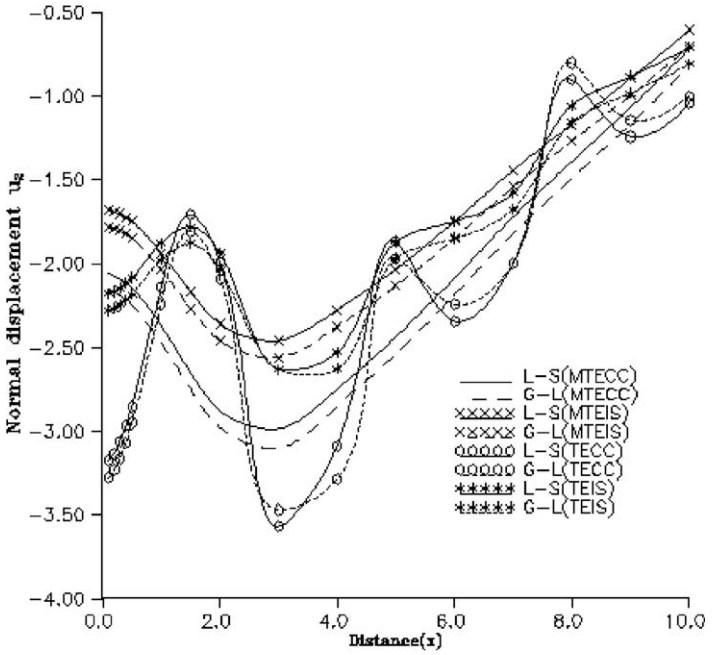

Fig. 33. Variation of normal displacement u_2 with distance x at $t = 0.25$. (Linearly distributed force; insulated boundary.)

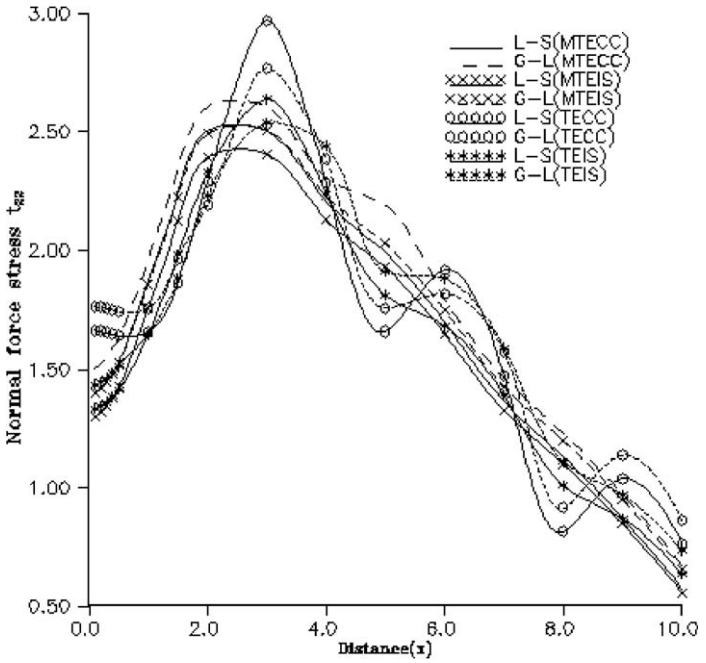

Fig. 34. Variation of normal force stress t_{22} with distance x at $t = 0.25$. (Linearly distributed force; insulated boundary.)

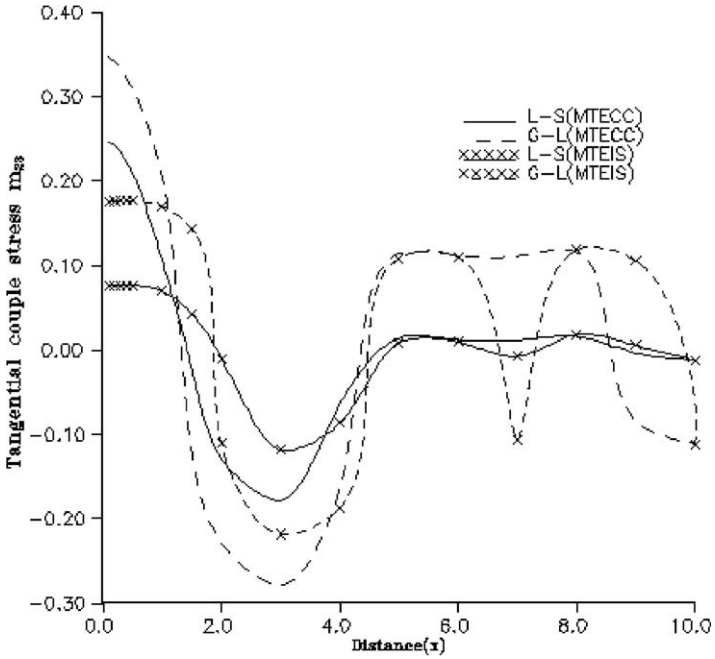

Fig. 35. Variation of tangential couple stress m_{23} with distance x at $t = 0.25$. (Linearly distributed force; insulated boundary.)

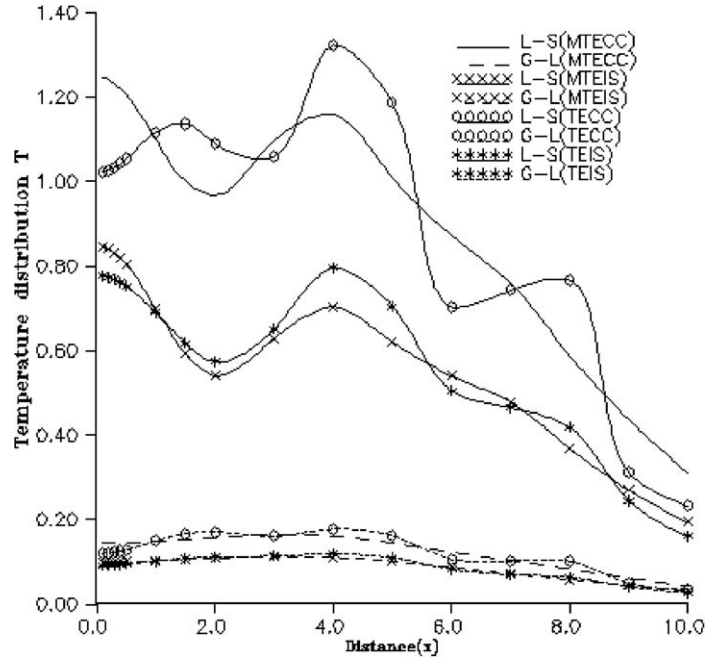

Fig. 36. Variation of temperature distribution T with distance x at $t = 0.25$. (Linearly distributed force; insulated boundary.)

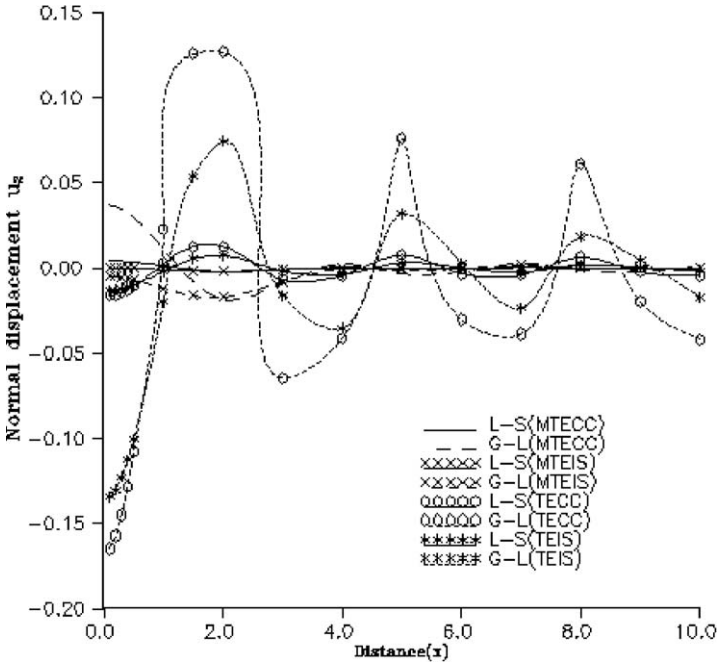

Fig. 37. Variation of normal displacement u_2 with distance x at $t = 0.25$. (Concentrated thermal source; insulated boundary.)

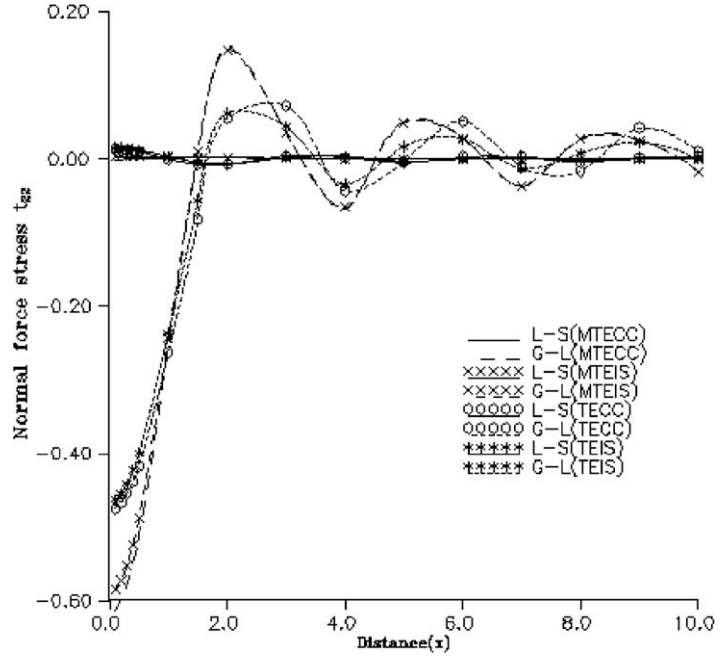

Fig. 38. Variation of normal force stress t_{22} with distance x at $t = 0.25$. (Concentrated thermal source; insulated boundary.)

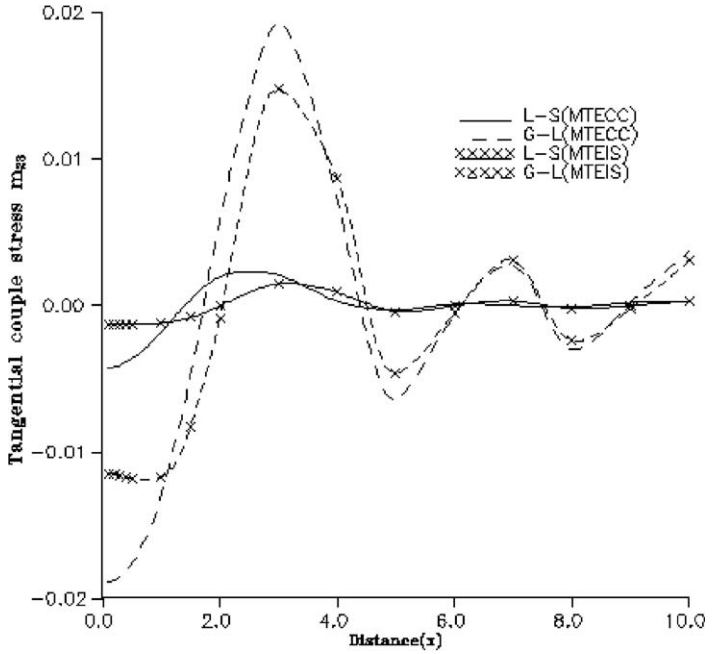

Fig. 39. Variation of tangential couple stress m_{23} with distance x at $t = 0.25$. (Concentrated thermal source; insulated boundary.)

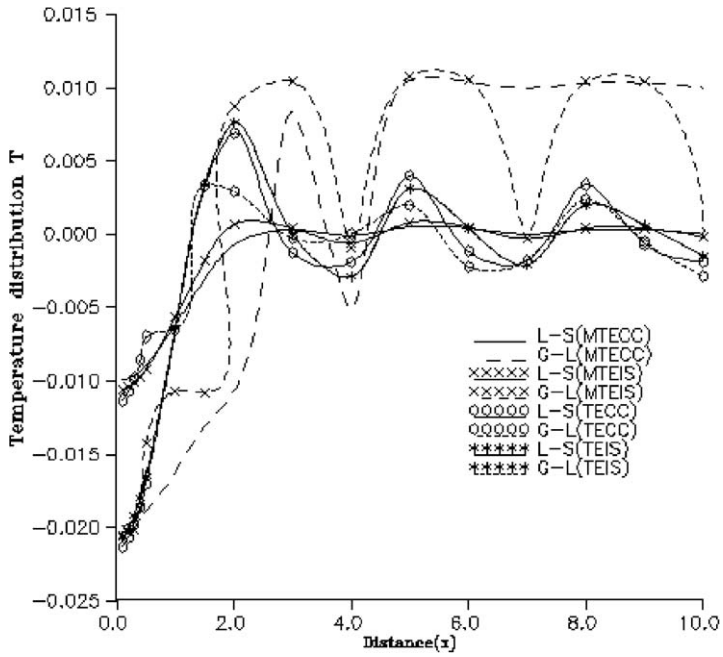

Fig. 40. Variation of temperature distribution T with distance x at $t = 0.25$. (Concentrated thermal source; insulated boundary.)

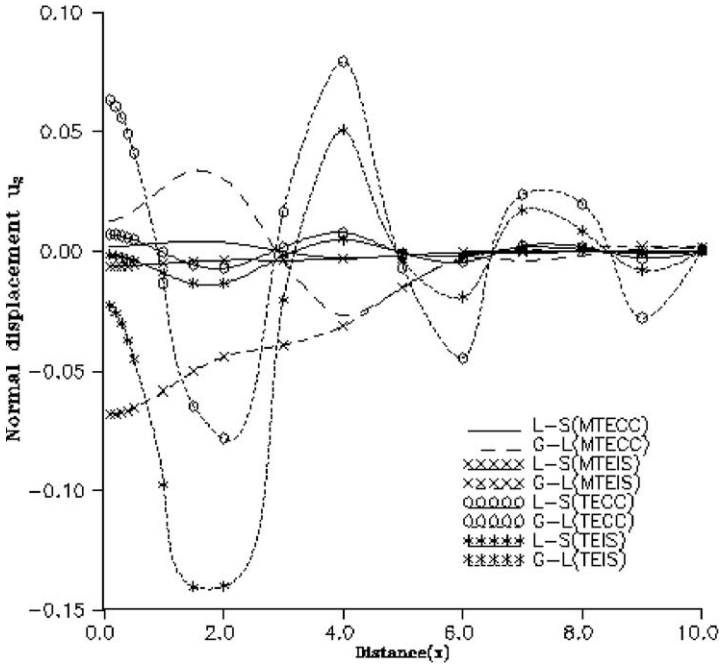

Fig. 41. Variation of normal displacement u_2 with distance x at $t = 0.25$. (Uniformly distributed thermal source; insulated boundary.)

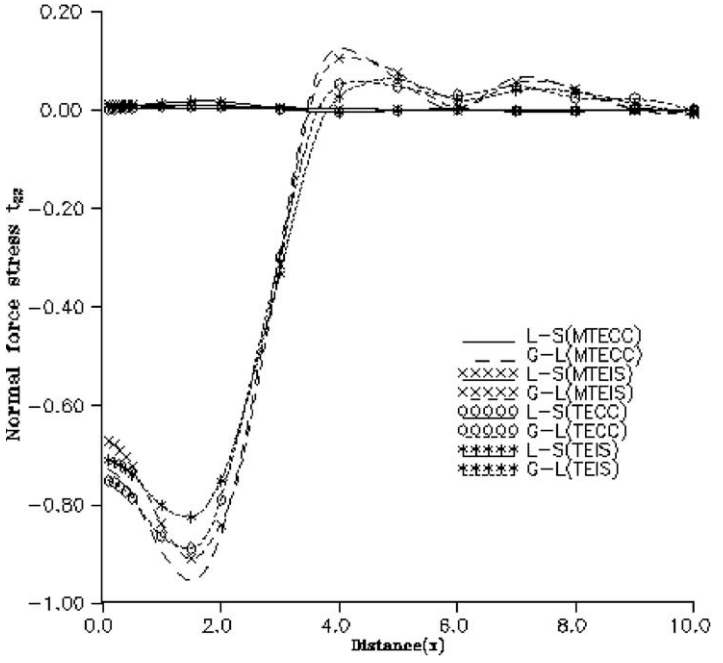

Fig. 42. Variation of normal force stress t_{22} with distance x at $t = 0.25$. (Uniformly distributed thermal source; insulated boundary.)

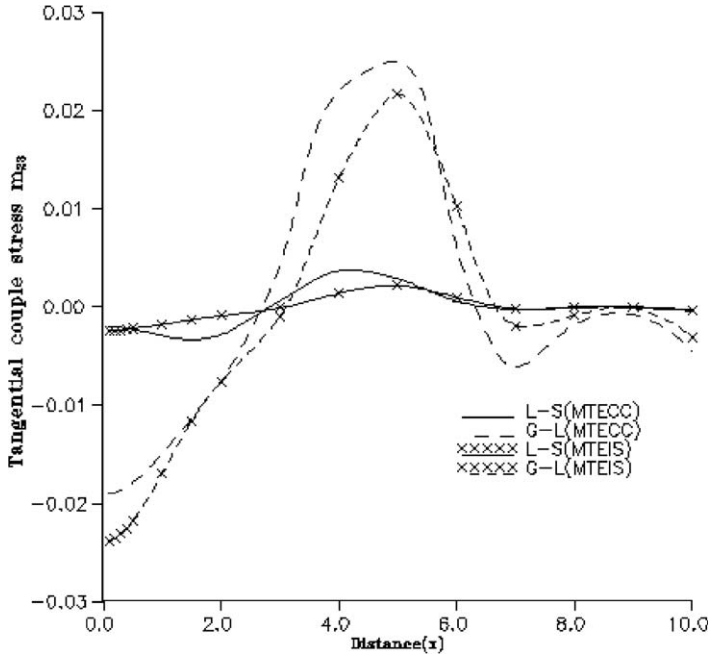

Fig. 43. Variation of tangential couple stress m_{23} with distance x at $t = 0.25$. (Uniformly distributed thermal source; insulated boundary.)

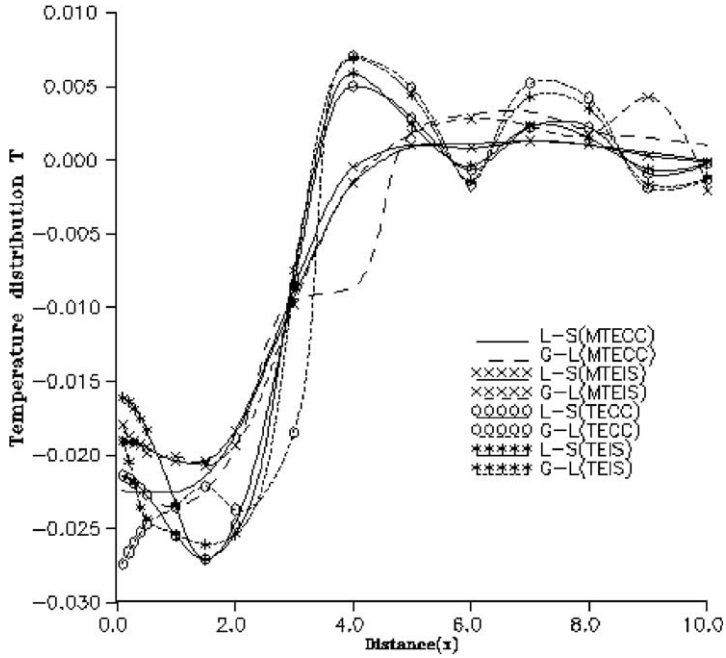

Fig. 44. Variation of temperature distribution T with distance x at $t = 0.25$. (Uniformly distributed thermal source; insulated boundary.)

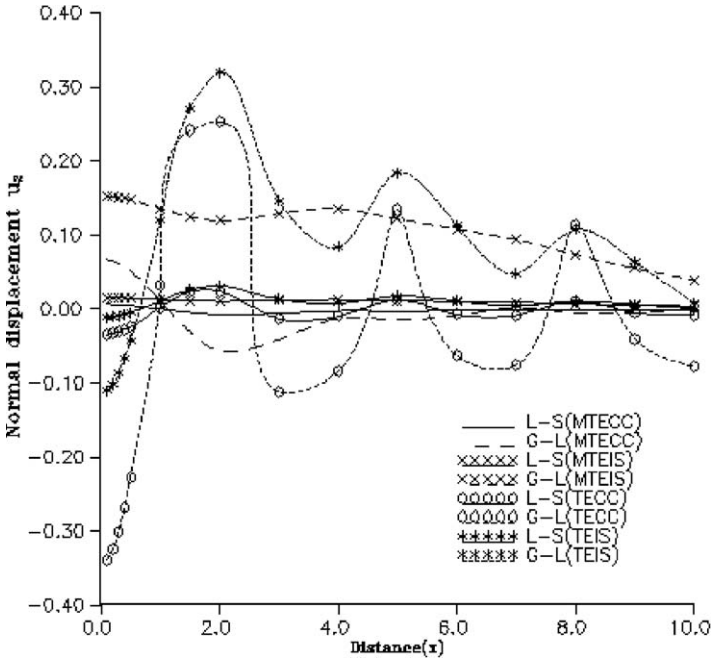

Fig. 45. Variation of normal displacement u_2 with distance x at $t = 0.25$. (Linearly distributed thermal source; insulated boundary.)

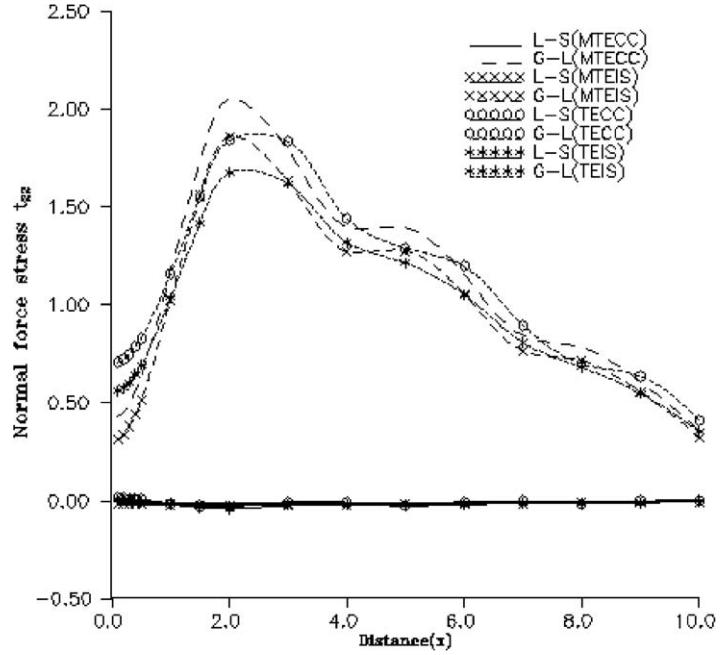

Fig. 46. Variation of normal force stress t_{22} with distance x at $t = 0.25$. (Linearly distributed thermal source; insulated boundary.)

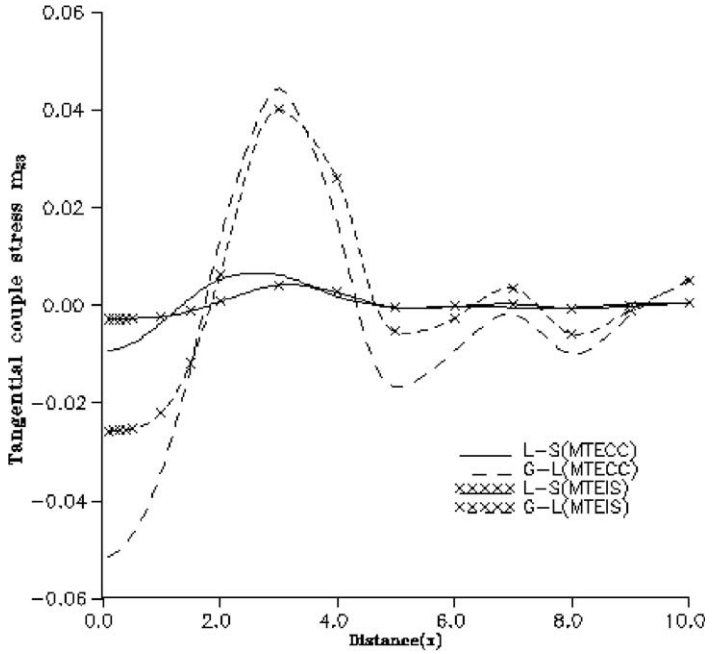

Fig. 47. Variation of tangential couple stress m_{23} with distance x at $t = 0.25$. (Linearly distributed thermal source; insulated boundary.)

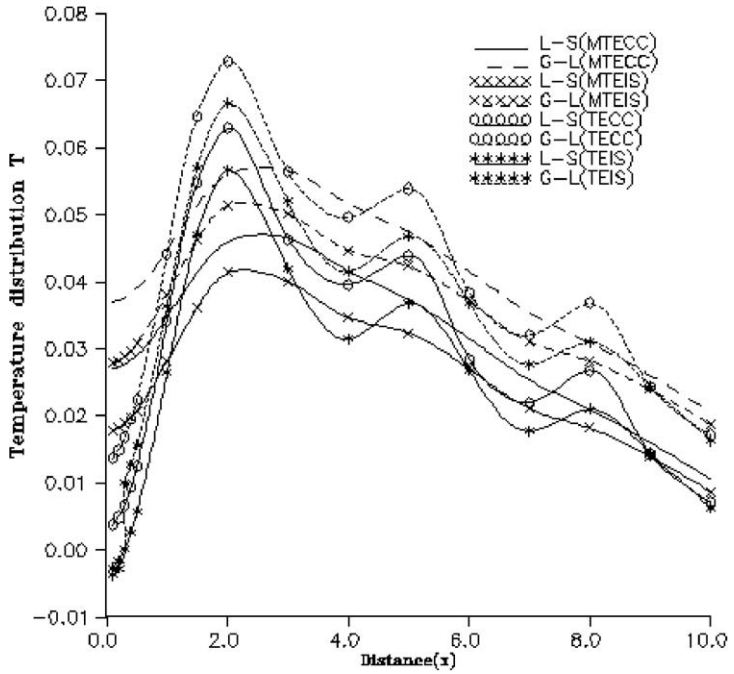

Fig. 48. Variation of temperature distribution T with distance x at $t = 0.25$. (Linearly distributed thermal source; insulated boundary.)

7. Discussions for various cases

7.1. Mechanical sources at $t = 0.1$

7.1.1. Concentrated forced

The values of normal displacement for MTECC and MTEIS are very close to each other (separately) for L–S and G–L theories. Also, these values lie in a very short range. The variations of normal displacement for the classical theory of thermoelasticity are more oscillatory. The values for TECC increase sharply and then oscillates with increase in horizontal distance x. These variations of normal displacement are shown in Fig. 1. The variations of normal force stress for micropolar theory of thermoelasticity are similar in nature to the variations of normal displacement. Also, the variations for classical theory of thermoelasticity are more oscillatory, but unlike the variations obtained for normal displacement, the values of normal force stress for both TECC and TEIS first decreases and then rises sharply to oscillate with increase in horizontal distance. These variations of normal force stress are shown in Fig. 2.

It is observed from Fig. 3 that very close to the point of application of source, the value of tangential couple stress is more for MTECC in comparison to the value for MTEIS. For any solid, the values of tangential couple stress for L–S and G–L theories are quite close to each other. It is interesting to note that the values of temperature distribution for G–L theory lie in a very short range for both the theories in comparison to the values for L–S theory. These variations of temperature distribution for both the theories have been shown in Fig. 4.

7.1.2. Uniformly distributed force

The variations of all the quantities of the solid for the micropolar theory of thermoelasticity are similar in nature to the variations obtained in case of concentrated normal force with difference in magnitudes. However, in the case of the classical theory of thermoelasticity, the variations of the quantities are less oscillatory in comparison to the variations in the previous case. These variations of normal displacement, normal force stress, tangential couple stress and temperature distribution are shown in Figs. 5–8, respectively.

7.1.3. Linearly distributed force

The values of normal displacement and normal force stress of solid lie in a short range for the micropolar theory of thermoelasticity. These values are very close for both L–S and G–L theories. But the variations for classical theory of thermoelasticity are oscillatory to a large extent as compared to the oscillations for micropolar theory. These variations of normal displacement and normal force stress are shown in Figs. 9 and 10, respectively. The variations of tangential couple stress for both MTECC and MTEIS are similar in nature with different magnitude. Also, these variations are similar to the variations obtained in the case of concentrated normal force. These variations of tangential couple stress are shown in Fig. 11.

It is observed from Fig. l2 that the values of temperature distribution for both micropolar and classical theories of thermoelasticity increase in the range $0.0 \leqslant x \leqslant 2.0$ and then decrease sharply with horizontal distance x. Since the values of temperature distribution are greater for L–S theory than for G–L theory, this decrease appears to be sharper for L–S theory, i.e., the values of temperature distribution for G–L theory lie in a short range.

7.2. Thermal sources at $t = 0.1$

7.2.1. Concentrated normal source

It is interesting to observe from Figs. 13 and 14 that the variations of normal displacement and normal force stress, respectively, are opposite in nature. Also the difference between the values of these quantities for L–S and G–L theories are very significant in comparison to the values obtained in case of mechanical sources where the difference is less significant. The variations obtained in this case are more uniform in nature. The values of tangential couple stress for L–S theory lie in a short range and hence are less oscillatory than the variations for G–L theory. These variations for tangential couple stress are shown in Fig. 15.

The variations of temperature distribution for both the theories increases initially in the range $0.0 \leqslant x \leqslant 2.0$ and then oscillates with horizontal distance x. These variations are smooth in nature for micropolar theory of thermoelasticity. The variations of temperature distribution in case of concentrated thermal source are shown in Fig. 16.

7.2.2. Uniformly distributed and linearly distributed thermal source

At any point in the range $0.0 \leqslant x \leqslant 10.0$ there is vast difference between the values of normal displacement, normal force stress and tangential couple stress for L–S and G–L theories in case of micropolar theory of thermoelasticity which is not the case in classical theory of thermoelasticity. Hence microrotation plays a vital role in the study of deformation of a body. These variations of normal displacement, normal force stress, and tangential couple stress for micropolar and classical theories of thermoelasticity are shown in Figs. 17–22, respectively, for uniformly distributed and linearly distributed thermal sources.

The discussions given above are, however, opposite in nature when we observe the results for temperature distribution. The values for L–S and G–L theories are close to each other for a particular solid. These variations of temperature distribution are shown in Figs. 23 and 24 for uniformly distributed and linearly distributed thermal source, respectively.

7.3. Mechanical sources at $t = 0.25$

7.3.1. Concentrated force

The variations of normal displacement, normal force stress, and tangential couple stress are similar in nature to the variations obtained at time $t = 0.1$, with different magnitude. But it is observed that the difference in values of normal displacement and tangential couple stress for L–S and G–L theories is more significant than the values obtained at time $t = 0.1$. These variations of normal displacement, normal force stress, and tangential couple stress for time $t = 0.25$ are shown in Figs. 25–27, respectively.

Similar to the variations obtained at time $t = 0.1$, the variations of temperature distribution for G–L theory lie in a short range. But the difference lies in the variations for L–S theory. While the variations of temperature distribution for both the theories at time $t = 0.1$ are uniform in nature, this is not the case at time $t = 0.25$. These variations of temperature distribution are shown in Fig. 28.

7.3.2. Uniformly distributed force

The variations of all the quantities are similar in nature, with difference in magnitude, to the variations obtained at time $t = 0.1$. These variations of normal displacement, normal force stress, tangential couple stress, and temperature distribution are shown in Figs. 29–32 respectively. Still, it is observed that the values of normal displacement and normal force stress obtained in this case for the micropolar and classical theories of thermoelasticity are close to each other as compared to the variations obtained at time $t = 0.1$.

7.3.3. Linearly distributed force

The variations of normal displacement and normal force stress for the micropolar theory of thermoelasticity (i.e., MTECC and MTEIS) and the classical theory of thermoelasticity (TECC and TEIS) are similar in nature separately. However, the variations are more oscillatory for the classical theory of thermoelasticity. These variations of normal displacement and normal force stress at time $t = 0.25$ are shown in Figs. 33 and 34 respectively.

It is observed from Fig. 35 that the variations of tangential couple stress for MTECC and MTEIS are similar in nature for both L–S and G–L theories separately. The variations of temperature distribution, shown in Fig. 36, depict that the variations for G–L theory (for both micropolar theory of thermoelasticity and classical theory of thermoelasticity) lie in a short range and these variations for L–S theory are oscillatory in nature for the solid.

7.4. Thermal sources at $t = 0.25$

7.4.1. Concentrated thermal source

Very similar to the variations of normal displacement, normal force stress, and tangential couple stress obtained at time $t = 0.1$, the values of these quantities are very small for G–L theory as compared to the values for L–S theory. This similarity is closer in the cases of normal force stress and tangential couple stress. These variations of normal displacement, normal force stress, and tangential couple stress are shown in Figs. 37–39, respectively. After observing Fig. 40, it can be said about the variations of temperature distribution that the difference in the values among L–S and G–L theories is very significant at time $t = 0.25$, whereas at $t = 0.1$ this difference is much less.

7.4.2. Uniformly distributed and linearly distributed thermal source

The variations of all the quantities are similar in nature to the variations obtained at time $t = 0.1$, with difference in magnitudes of the values. While the variations of normal displacement, normal force stress, tangential couple stress, and temperature distribution for uniformly distributed thermal sources are shown in Figs. 41–44, the variations of these quantities for linearly distributed thermal sources are shown in Figs. 45–48, respectively.

8. Conclusions

The properties of a body depend largely on the direction of symmetry. A significant micropolarity effect is observed on all the quantities. When concentrated force is applied on the surface of a solid, the variations of normal displacement and normal force stress for the micropolar theory of thermoelasticity are less oscillatory, than for the classical theory of thermoelasticity, while in the case of temperature distribution the variations are opposite in nature for the two theories. The variations of all the quantities for L–S and G–L theories are quite close to each other. Also the variations of tangential couple stress for concentrated force, uniformly distributed force, and linearly distributed force are similar in nature. On application of thermal source on the boundary, the difference between the values of normal displacement, normal force stress, and tangential couple stress for L–S and G–L theories are very significant.

References

Bertram, A., Bohlke, T., Gaffke, N., Heiligers, B., Offinger, R., 2000. On the generation of discrete isotropic orientation distributions for linear elastic cubic crystals. J. Elast. 58 (3), 233–248.

Boulanger, P., Hayes, M., 2000. Special inhomogeneous plane waves in cubic elastic materials. Z. Angew. Math. Phys. 51, 1031–1038.

Chung, D.H., Buessem, W.R., 1967. The elastic anisotropy of crystals. J. Appl. Phys. 38 (5), 2010–2012.

Destrade, M., 2001. The explicit secular equation for surface acoustic waves in monoclinic elastic crystals. J. Acoust. Soc. Am. 109 (4), 1398–1402.

Dhaliwal, R.S., Singh, A., 1980. Dynamic Coupled Thermoelasticity. Hindustan Publication Corporation, New Delhi, India, p. 726.

Domanski, W., Jablonski, T., 2001. On resonances of nonlinear elastic waves in a cubic crystal. Arch. Mech. 53 (2), 91–104.

Eringen, A.C., 1966. Linear theory of micropolar elasticity. J. Math. Mech. 15, 909–923.

Eringen, A.C., 1984. Plane waves in non-local micropolar elasticity. Int. J. Eng. Sci. 22, 1113–1121.

Green, A.E., Lindsay, K.A., 1972. Thermoelasticity. J. Elast. 2, 1–5.

Green, A.E., Naghdi, P.M., 1991. A re-examination of the basic postulates of thermomechanics. Proc. R. Soc. London Ser. A 432, 171–194.

Honig, G., Hirdes, V., 1984. A method for the numerical inversion of the Laplace transform. J. Comput. Appl. Math. 10, 113–132.

Kobayashi, R., Giga, Y., 2001. On anisotropy and curvature effects for growing crystals. Jpn. J. Ind. Appl. Math. 18 (2), 207–230.

Kumar, R., Choudhary, S., 2002a. Influence and Green's function for orthotropic micropolar continua. Arc. Mech. 54, 185–198.

Kumar, R., Choudhary, S., 2002b. Dynamical behavior of orthotropic Micropolar elastic medium. J. Vib. Control 8, 1053–1069.

Kumar, R., Choudhary, S., 2003. Response of orthotropic micropolar elastic medium due to various sources. Meccanica 38, 349–368.

Kumar, R., Rani, L., 2003. Elastodynamics of time harmonic sources in a thermally conducting cubic crystal. Int. J. Appl. Mech. Eng. 8 (4), 637–650.

Lie, K-H.C., Koehler, J.S., 1968. The elastic stress field produced by a point force in a cubic crystal. Adv. Phys. 17, 421–478.

Lord, H.W., Shulman, Y., 1967. A generalized dynamical theory of thermoelasticity. J. Mech. Phys. Solids 15, 299–306.

Minagawa, S., Arakawa, K., Yamada, M., 1981. Dispersion curves for waves in a cubic micropolar medium with reference to estimations of the material constants for diamond. Bull. JSME 24 (187), 22–28.
Press, W.H., Teukolsky, S.A., Vellerling, W.T., Flannery, B.P., 1986. Numerical Recipes. Cambridge Univ. Press, Cambridge, UK.
Steeds, J.W., 1973. Introduction to Anisotropic Elasticity Theory of Dislocations. Clarendon Press, Oxford.
Zhou, F., Ogawa, A., 2002. Elastic solutions for a solid rotating disk with cubic anisotropy. ASME J. Appl. Mech. 69, 81–83.